DOT/FAA/AR-99/22

Office of Aviation Research
Washington, D.C. 20591

The Effect of Loading Parameters on Fatigue of Composite Laminates: Part III

June 1999

19990805 025

Final Report

This document is available to the U.S. public
Through the National Technical Information
Service (NTIS), Springfield, Virginia 22161.

U.S. Department of Transportation
Federal Aviation Administration

DTIC QUALITY INSPECTED 2

NOTICE

This document is disseminated under the sponsorship of the U.S. Department of Transportation in the interest of information exchange. The United States Government assumes no liability for the contents or use thereof. The United States Government does not endorse products or manufacturers. Trade or manufacturer's names appear herein solely because they are considered essential to the objective of this report. This document does not constitute FAA certification policy. Consult your local FAA aircraft certification office as to its use.

This report is available at the Federal Aviation Administration William J. Hughes Technical Center's Full-Text Technical Reports page: www.tc.faa.gov/its/act141/reportpage.html in Adobe Acrobat portable document format (PDF).

1. Report No. DOT/FAA/AR-99/22	2. Government Accession No.	3. Recipient's Catalog No.
4. Title and Subtitle THE EFFECT OF LOADING PARAMETERS ON FATIGUE OF COMPOSITE LAMINATES: PART III		5. Report Date June 1999
		6. Performing Organization Code
7. Author(s) H. Thomas Han, Milan Mitrovic, and Ozgur Turkgenc		8. Performing Organization Report No.
9. Performing Organization Name and Address Mechanical and Aerospace Engineering Department Engineering IV University of California Los Angeles, CA 90024-1597		10. Work Unit No. (TRAIS)
		11. Contract or Grant No. DTFA03-92-A-00003
12. Sponsoring Agency Name and Address U.S. Department of Transportation Federal Aviation Administration Office of Aviation Research Washington, DC 20591		13. Type of Report and Period Covered Final Report
		14. Sponsoring Agency Code AIR-120

15. Supplementary Notes

The William J. Hughes Technical Center Monitor was Peter Shyprykevich.

16. Abstract

The long-term mechanical fatigue of quasi-isotropic graphite/epoxy laminates was investigated to determine the influence of loading parameters on impact-induced delamination growth during constant-amplitude and spectrum fatigue loading. Based on the test results, recommendations for fatigue design of composite laminates in the presence of barely visible impact damage (BVID) are suggested.

17. Key Words Graphite/epoxy, Impact damage, Spectrum loading, Damage tolerance, Delamination, Load sequence	18. Distribution Statement This document is available to the public through the National Technical Information Service (NTIS), Springfield, Virginia 22161.		
19. Security Classif. (of this report) Unclassified	20. Security Classif. (of this page) Unclassified	21. No. of Pages 69	22. Price

Form DOT F1700.7 (8-72)   Reproduction of completed page authorized

TABLE OF CONTENTS

LIST OF FIGURES

iv

LIST OF TABLES

LIST OF ABBREVIATIONS AND SYMBOLS

L	Delamination length
a, b, c	Best-fit parameters
m_i	Coefficients in power law for delamination growth
n_i	Exponent in power law for delamination growth
G	Strain energy release rate
G_c	Critical value of G at delamination onset
N	Number of fatigue cycles
R	Fatigue cyclic stress ratio (S_{min}/S_{max})
S-N	Strength versus number of cycles curves
S	Cyclic stress
ΔS	Cyclic stress range ($S_{max} - S_{min}$)
S_{max}	Maximum stress of fatigue cycle
S_{min}	Minimum stress of fatigue cycle
f	Cyclic frequency
BVID	Barely visible impact damage
C.A.	Constant-amplitude fatigue loading
C-C	Compression-compression fatigue loading
T-C	Tension-compression fatigue loading
T-T	Tension-tension fatigue loading
CSAI	Compressive strength after impact
RCS	Residual compressive strength (after post-impact fatigue)
UCS	Ultimate compression strength
FML	Flight mean load in spectrum fatigue
FALSTAFF	Fighter Aircraft Loading STAndard For Fatigue load spectrum
TWIST	Transport WIng Standard Test Spectrum

EXECUTIVE SUMMARY

This report is the third in a continuing series of reports that will provide comprehensive documentation of damage induced by spectrum fatigue loading in composite laminates and its influence on residual mechanical properties. The overall study will delineate the effects of component parts of the load spectrum on fatigue damage development and provide recommendations for fatigue design of composite laminates and accelerated testing methodology. This report focuses on the delamination growth behavior in composite laminates containing barely visible impact damage under different fatigue loading conditions.

Quasi-isotropic $[0/+45/-45/90]_{s4}$ laminates made from an AS4/3501-6 graphite/epoxy material system were used in this study. Initial impact tests were performed to determine the influence of impact test parameters on damage development and its influence on compressive-strength reduction. Impact parameters were adjusted to produce barely visible impact damage for subsequent fatigue loading. Influence of fatigue loading parameters on damage growth in the form of delamination was recorded under the constant-amplitude, block, and spectrum loading. Following the fatigue testing, static compression tests were performed to assess the effect of fatigue-generated damage on residual compressive strength.

Experimental results from tension-tension and tension-compression fatigue of specimens containing barely visible impact damage show negligible differences in terms of life and damage propagation modes when compared to undamaged specimens. Constant-amplitude compression-compression loading tests indicate that the impact-induced delamination grows only after the separation of the thin delaminated region, located on the rear impacted side, from the base laminate. This delamination failure does not occur at load levels below 60% of the CSAI (compressive strength after impact). However, following the high load excursions (>70% CSAI) which initiate damage growth, delamination propagation due to local buckling is observed even when the minimum compressive stress is reduced to 30% CSAI. Two-level block-loading tests indicate that for this type of damage, high/low loading sequence is more detrimental than the low/high loading sequence. Qualitative trends in the experimental data generated by compression-dominated spectrum loading tests are shown to be similar to the fatigue behavior under the constant-amplitude and two-level block loading. Observed impact damage growth during these tests suggest that the two lowest load levels (which represent 98.69% of the whole spectrum) can be deleted from the test sequence without significant influence on impact damage propagation. That is, durability testing can be accelerated by omitting those cycles whose load range (ΔS) is equal or less than 20% CSAI. Residual compressive strength measurements conducted on specimens subjected to compression-dominated fatigue indicate that this material property is not sensitive to subcritical damage which forms during fatigue (i.e., delaminations that span only a few surface plies).

1. INTRODUCTION.

One of the obstacles to wider application of composites in aircraft structures is the difficulty in certifying composite structures. Being fairly new, composites do not yet enjoy the kind of databases that conventional materials do. Thus, certification requires lengthy testing of elements and components under realistic loading environments. It therefore makes economic sense to modify the loading spectrum to reduce testing time as much as possible.

The main goal of the present study is to delineate the effects of various parameters defining spectrum loading on damage growth. Once these effects are identified, one can accelerate fatiure testing by changing appropriate loading parameters. The first two reports [1,2] addressed the effects of preload, block loading, stress ratio, and loading frequency on damage development in plain coupons and specimens with a stress raiser in the form of a centrally located hole. This report addresses damage propagation in composite laminates containing barely visible impact damage under different fatigue loading conditions.

The objective of the current study is to determine the influence of loading parameters on impact-induced delamination growth in composite laminates containing barely visible impact damage during fatigue loading. Specifically, the effects of load type, load level, load sequence, as well as the effects of spectrum modification were studied. In the following sections, experimental results are presented and discussed to identify these effects. Analytical studies were also performed to identify the governing damage growth parameters, with the aim of extending current experimental observations to different material systems and impact loading conditions. A finite element analysis coupled with a fracture mechanics approach was used in this study, with the assumption that delamination growth is governed by strain energy release rates. Based on experimental and analytical results, a method to accelerate fatigue testing of impacted composite laminates by selecting appropriate loading parameters is suggested.

2. BACKGROUND.

In aircraft applications, composite panels are routinely subjected to both low-velocity impacts and long-term mechanical loading (fatigue). These loading events cause damage to develop in the form of fiber breakage, matrix microcracking, and delaminations which lead to material property degradation with the most severe being in compression strength. This reduction raises serious concerns about using composite components in critical locations of aircraft which must provide support for compressive loads during normal operation, and it represents one of the major issues for satisfying the safety requirements of aircraft structures. An overview of the work done by other researchers aimed at characterizing and predicting the impact damage growth in composite materials during various loading scenarios is presented in the following sections. Parameters that affect damage initiation and accumulation during impact and fatigue loading are examined, together with the influence of various damage states on the residual mechanical properties and strength.

1

2.1 LOW-VELOCITY IMPACT DAMAGE AND RESIDUAL STRENGTH.

Low-velocity impact damage causes fiber breakage, matrix cracking, and delaminations. The plies on the face opposite the impact site have more matrix cracking and delaminations due to the higher bending stresses in the plies at that location. At the point of contact with the impactor, fiber breakage typically occurs, which can substantially reduce the tensile strength of the specimen. However, while low-velocity impact causes a fairly complicated damage pattern, the dominant damage mode for this type of loading is the formation of single or multiple delaminations between the plies of the laminate.

During the impact event, a strong interaction arises between matrix cracking and delamination. The growth rate of the delamination will decrease during the loading process when a matrix crack is encountered. That is, during impact the delamination starts at the tip of the first crack and grows fast until another crack is formed and other delaminations start from the tips of newly formed cracks [3]. In general, once a delamination is initiated from a matrix crack, it grows much more extensively along the fiber direction of the bottom layer at the interface following the contours of interlaminar shear stresses σ_{xz} and σ_{yz}, which explains the characteristic peanut shape of delamination observed by different researchers [4].

Depending on the type and extent of damage, the residual strength of impacted composite plates can be reduced significantly. Influence of delamination on the degradation of residual compressive strength has been well documented in the literature [5-15]. However, delamination as the predominant impact damage pattern does not influence tensile strength significantly, but the fiber breakage and associated stress concentration do. Cairns and Lagace [16] reported a 50% reduction in the residual tensile strength for a 14-mm damage diameter indicative of fiber breakage (for 70-mm-wide specimens). They have also concluded that the residual strength is not an explicit function of impact energy but is soley a function of the damage present. That is, the damage was inflicted with different impactor mass, velocity, and boundary conditions, but for the equivalent damage an equivalent strength performance was observed. Therefore, impact energy may not be an accurate parameter to predict residual properties.

2.2 POST-IMPACT FATIGUE BEHAVIOR.

The post-impact fatigue behavior has been studied by a few researchers on different materials, lay-ups, and for different loading conditions. Stellbrink [12] studied the fatigue behavior under the tension-compression (T-C) loading (R = -1, f = 5 Hz) of T300/69 and T300/914 quasi-isotropic laminates. Initial impact damage corresponded to a 200-400 mm² area in the form of a delamination and 20-90 mm² of visible damage at the rear (for 250- x 50-mm specimens). Tensile strength was not reduced significantly, while the compressive strength was reduced by ~50%. From the established S-N curves, it was concluded that the rate of life reduction is higher for undamaged than for damaged specimens and that test data agree better with the sudden death model than with the degradation model.

The influence of impact damage on the fatigue behavior of AS4/3501-6 [+45/-45/0/0/+45/-45/0/0/+45/-45/0/90]$_{2S}$ laminates under tension-tension (T-T), T-C, and compression-compression (C-C) loading was studied by Ramkumar [13]. Two types of low-velocity impacts

with ~5 cm in delamination diameter were investigated with (sharp impactor—type II) and without (blunt-tipped impactor—type I) visible damage on the outer surfaces of laminates. The specimen gage length was 13 x 15 cm, requiring the use of antibuckling devices for compressive loads. Type I damage caused a 20% reduction in static tensile strength and a 65% reduction in the compressive strength, while the type II damage caused a 42% reduction in the tensile strength and a 67% reduction in the compressive strength. Fatigue testing was performed at stress levels above 60% of ultimate tensile strength (UTS) ultimate compressive strength (UCS), and while most of the specimens subjected to T-T loading survived 1 million cycles, all specimens loaded in T-C and C-C failed well before. The author indicated that tensile loading, static or fatigue, represents the least threat to impact damaged laminates. Overall damage propagation was monitored by ultrasonic pulse-echo transducer and C-scan, and for the laminates investigated, damage growth for compression-dominated loading was reported to be in the direction perpendicular to the loading direction.

In another experimental study by Ramkumar [14], the effect of embedded (idealized) delaminations on the compression behavior of three different stacking sequences of quasi-isotropic T300/5208 graphite/epoxy laminates was investigated. From the *S-N* data, it was concluded that the threshold value of the maximum compressive stress, at which failure is not expected to occur, depended on the location and shape of implanted delamination. Also, the occurrence of delamination growth and its direction was shown to be dependent on the laminate stacking sequence and its through-the-thickness location. Failures were induced predominantly when the embedded delaminations grew to the tab region. The significance of the stacking sequence on delamination growth and failure modes in notched composite laminates has also been pointed out by Ratwani and Kan [17]. They indicated that damage may propagate along the loading direction, or in a direction at some angle to the loading direction, depending on the stacking sequence. The location of the delamination appeared to coincide with positions of highest interlaminar shear or normal stresses as predicted by a finite element analysis.

Blaricum et al. [15] studied the compression dominated loading on [+45/-45/0/0/]$_{7S}$ XAS-914C specimens with impact damage loaded using the modified Fighter Aircraft Loading STAndard for Fatigue (FALSTAFF) load spectrum flight-by-flight sequence (300 x 100 mm). Fatigue testing was performed under a maximum compressive strain of 0.36%. It was reported that for this type of material and lay-up, the low load levels could be deleted from the testing sequence with no significant effect on fatigue life and that the effect of duration of high-level loads (0.12 and 10 seconds) did not influence fatigue life significantly. Damage growth rate as a function of the initial damage width was monitored, and it appeared that the damage width was a major controlling factor in these tests. The authors suggested that a consistent and clearly defined damage growth behavior could be derived from a number of tests.

Some researchers also suggested that impacted composite panels have very flat compression *S-N* curves (Demuts et al. [18]) and that although compression strength is greatly influenced by impact damage, any subsequent reduction under fatigue loading is minimal (O'Brien [19]). This contradicts the observations of Ramkumar [14], as discussed earlier, suggesting that a more accurate characterization of damage tolerance criteria for impact-damaged composite laminates is needed.

3

2.3 PREDICTION OF DELAMINATION GROWTH UNDER STATIC LOADING.

Modeling of delamination growth under compression loading and prediction of the residual compressive strength of impacted specimens has been a topic of a number of studies. In a series of papers, Whitcomb [20-22] analytically investigated delamination growth caused by local buckling of a delaminated group of plies. Through-width delamination was studied under uniaxial and biaxial compressive loads, and the delamination growth was assumed to be governed by the strain energy release rates G_I, G_{II}, and G_{III}. The effect of the delamination shape and size on the strain energy release rate distribution along the delamination front was analyzed using a geometrically nonlinear finite element model. It was reported that the problem was a mixed mode one, with the locations of maximum G_I and G_{II} depending on the delamination shape (circular or elliptical) and the applied strain, with a negligible contribution from mode III. Also, large gradients in the strain-energy release rates along the delamination front were found, suggesting different directions of delamination growth depending on the choice of growth criterion. For embedded circular delamination under uniaxial compression, the growth was suggested to occur perpendicular to the loading direction, indicating a change into an elliptical shape. However, for an elliptical delamination the peak values for G_{II} were found to be parallel to the loading direction, while the location of maximum values for G_I did not change, suggesting almost uniform growth along the delamination front.

Compression failure of laminated composites containing artificially implanted multiple delaminations has been studied analytically and experimentally by Kutlu and Chang [23]. A two-dimensional nonlinear finite element model which simulates the compression response, from initial loading to the final collapse, of laminated composites containing multiple through-the-width delaminations was developed by the authors. The failure analysis was based on the principles of fracture mechanics for predicting delamination growth and the Hashin failure criteria combined with the material degradation rules for predicting the occurrence and mode of failure. Based on the results of this analysis it was suggested that the buckling and subsequent postbuckling response of the sublaminates triggers the delamination growth and that the residual thermal stresses may be important for accurate modeling of the postbuckling behavior.

2.4 SUMMARY.

Most of the research work to date on fatigue of composite laminates with impact induced damage has focused on the final failure and not on damage evolution. The objective of this research is to determine the influence of loading parameters on impact-induced delamination growth during fatigue loading and the fatigue design limits (delamination growth thresholds) for composite laminates containing barely visible, low-velocity impact damage. Specifically the effects of load type, load level, load sequence, the effect of overloads, and their magnitude and location in the load spectrum were of interest in this study. In the following sections, experimental results which identify these effects are presented and discussed. Based on the experimental results, a method to accelerate durability testing of impacted composite laminates by selecting appropriate loading parameters is suggested.

3. EXPERIMENTAL PROCEDURE.

Quasi-isotropic laminates made from an AS4/3501-6 graphite/epoxy material system were used in this study. Hercules AS4/3501-6 prepregs were cured in an autoclave according to the manufacturer's recommended cure cycle to fabricate 24-ply $[0/\pm45/90]_{S3}$ and a 32-ply $[0/\pm45/90]_{S4}$ panels. The nominal per ply thickness was taken as 0.005″. The actual panel thicknesses molded out to 0.12″ for 24-ply laminate and 0.18″ for the 32-ply laminate. Each panel measuring 914 mm by 406 mm was cut into six subpanels 305 mm by 203 mm and inspected using an ultrasonic C-scan system. The subpanels were then cut into test specimens of various dimensions depending on the test condition. The 24-ply panels were used in T-T fatigue while the thicker 32-ply panels were used in T-C and C-C fatigue to prevent specimen buckling.

3.1 IMPACT LOADING.

Impact tests were performed on a Dynatup 8200 drop weight impact testing machine with a 4.3-kg impactor having a 12.7-mm tup diameter. A modified SACMA SRM 2-88 [24] impact fixture was used to provide the necessary support for the specimens. A smaller 25.4- x 25.4-mm square cutout was used instead of the recommended 76.2- x 127-mm cutout (see figure 1) to accommodate the specimen dimensions used in this study. A model 730-I data acquisition and analysis system was used with the Dynatup 8200 drop weight impact testing machine. The capabilities of this instrumentation include complete records of energy and force as a function of time (GRC, Instruction Manual [25]). The energy calculations performed by the data acquisition system require the crosshead velocity at impact, which is obtained by measuring the time necessary for a flag of known width to pass through a light beam. The model 730-I uses a flag mounted on the crosshead and a photo-detector block on an adjustable bracket for this purpose. The impact velocity is computed from the time the velocity detector light beam is occluded to the time the light beam reestablishes itself. The impact hammer (tup) is also used to measure the force during the impact, i.e., load vs. time. By integrating the force versus time curve, and knowing the initial impact velocity, the energy history and the energy absorbed by the composite can be calculated.

3.2 STATIC AND FATIGUE TESTING.

Static and resudual compression tests were performed on a 500-kN capacity Instron test frame. The specimens were loaded at a displacement rate of 1.27 mm/min, per ASTM D3410-75 standard [26]. An end-loaded compression test fixture, similar to the NASA short-block compression test fixture (see figure 2) was used. As shown in figure 2, the test fixture consists of two steel plates, with two blocks attached to support the specimen at the ends. The blocks are bolted to the steel plates and provide sufficient support to prevent end brooming of the specimen. The test fixture was placed in the test frame on a spherical seat to align the specimen during compression. Following static tests, fatigue testing was performed on a 100-kN capacity Instron test frame. A gage length of 38.1 x 38.1 mm was chosen for the coupons in static- and compression-dominated fatigue tests to prevent global buckling (see specimen dimensions in figure 2).

5

T-T, T-C, and C-C constant-amplitude and block-loading tests were performed (using tabbing material in the grip area) to determine the influence of different loading parameters on impact-induced damage growth. Also, compression-dominated spectrum loading was investigated using the standardized Transport Wing Standard Test (TWIST) spectrum. Damage progression was monitored periodically during fatigue using radiography. Additionally, some specimens were sectioned and inspected microscopically to determine the delamination growth on a ply-by-ply basis. Following the fatigue testing, static compression tests were performed on selected specimens to assess the influence of the additional damage caused by fatigue cycling on the residual compressive strength (RCS). The load levels selected for the fatigue testing were based on the static compressive strength after the impact (CSAI) event.

3.3 COMPRESSION-DOMINATED BLOCKED TWIST LOADING.

In this study the compression-dominated TWIST spectrum was used to determine the effect of the more severe mode of compression loading on delamination propagation. TWIST (table 1) consists of ten basic flights (A-J) which are repeated to make a single block of TWIST composed of 4,000 flights (Phillips [27] and Schütz [28]). Each flight consists of ten stress levels (1-10) ranging from 0.222 to 1.6 of flight mean load, such that a single block of TWIST consists of 398,665 cycles. The magnitude and the cumulative number of cycles per block for each load level present in ten basic flights are outlined in table 1. The occurrence of each load level within one flight and the flights within one block of TWIST is completely random. An example of a randomly generated loading sequence for the eight highest load levels from flight A is presented in figure 3 (top graph). However, instead of this type of loading sequence, a blocked loading in which the load levels are executed from the highest to the lowest one, was used in current tests (see figure 3 (bottom graph)). Note that all load excursions present in the randomly generated sequence are also included in the blocked loading sequence. Furthermore, each block is repeated 10 times, up to 40,000 flight hours, so that the loading sequence effect is still preserved. The reason for using this type of orderly loading sequence is that one can more clearly identify the influence of each load excursion on damage propagation. Most of the specimens in this study were inspected after the two highest load levels and again before the two lowest load levels within each block. Some specimens were inspected after completion of 2nd, 4th, 6th, 8th, and 10th load level within each block of TWIST.

4. ANALYTICAL MODELING.

While a number of researchers have investigated delamination growth using the concepts of linear elastic fracture mechanics [20-22, 29-32], the question of characterizing delamination growth under fatigue is still not well understood. Typically, delamination growth is assumed to be governed by strain energy release rates G_I, G_{II}, and G_{III}. In the present study a finite element computer code PATRAN was used to calculate energy release rates for a simulated delamination.

The actual initial impact damage has a circular shape with multiple delaminations throughout the thickness. To accurately model this type of damage a complete three-dimensional finite element model would be needed. However, the actual damage growth in fatigue more closely resembles a single delamination propagation front, rather than the growth of embedded multiple delaminations. This is schematically represented in figure 4, which shows a single through-width

6

delamination. Thus, an idealized plane-strain finite element model was used to determine mode I and mode II components of the strain energy release rate.

Based on radiographs of the impacted sample, the initial delamination was assumed to be 12 mm in length and one or two plies from the top surface. Homogenous quasi-isotropic laminate properties were used, and the mechanical properties for AS4/3501-6 graphite/epoxy material system are listed in table 2. Due to symmetry, only one quarter of the plate was modeled, figure 4, with the boundary conditions indicated in the figure. The delamination was modeled by disconnecting the nodes between the two sublaminates and placing gap elements between these nodes to prevent inadmissible overlap of sublaminates.

When subjected to a compressive load, the thin sublaminate buckles causing high interlaminar stresses at the delamination tip causing delamination growth. Hence, the influence of buckling and postbuckling of the sublaminate on delamination growth can be studied using a geometrically nonlinear static analysis. To initiate out-of-plane displacements an initial imperfection was assumed as

$$w_{max} = \cos\left(\frac{\pi x}{2a}\right) \tag{1}$$

where the maximum initial imperfection (w_{max}) is chosen to be 10% of the delaminated ply thickness (0.0125 mm). Strain energy release rates along the delamination front were determined using the modified crack closure technique (see Rybicki and Kanninen [33]), and the individual strain energy release rates, associated with the two modes of fracture, were determined from (Mukherjee et al. [34]):

$$G_I = \lim_{\Delta a \to 0} \frac{1}{2\Delta a} \int_0^{\Delta a} \sigma_{yy}(x)\Delta u_y(x+\Delta a)dx$$

$$\tag{2}$$

$$G_{II} = \lim_{\Delta a \to 0} \frac{1}{2\Delta a} \int_0^{\Delta a} \sigma_{xy}(x)\Delta u_x(x+\Delta a)dx$$

Figure 4 schematically shows the elements and nodes in the delamination front region. Relative displacements were obtained as differences between absolute displacements at nodes c_1 and c_2. The assumed change in crack length (Δa) was taken to be 1% of the total crack length (a), as suggested from convergence studies by other researchers (Jih and Sun [35]).

5. RESULTS AND DISCUSSION.

5.1 IMPACT DAMAGE EVALUATION.

Initial impact tests were performed to determine the influence of impact test parameters on damage development. Impact energy was adjusted to produce a barely visible impact damage for subsequent fatigue loading. The overall impact damage area, in the form of a delamination, was

7

determined using radiography and plotted versus the incident impact energy in figure 5 (see also table 3). Caution should be taken in assuming that the maximum damage diameter is 25.4 mm, since it coincides with the 25.4- x 25.4-mm square cutout of the clamping fixture. The damage area might have been larger if a larger clamping fixture had been used.

Specimens that were impacted with an incident energy of 1.9 Joules displayed a large variation in damage. Radiographs of some specimens showed damage ~12.7 mm in diameter, while others showed no damage at all. Furthermore, sectioning and microscopic examination of these specimens did not reveal any sign of damage. This variability may be attributed to the inconsistency in the experimental setup or that this value is near the damage threshold level. Slightly above this energy level the damage was consistent, ~12.7 mm in diameter, which corresponded to 33% of the specimen width. Thus, one may conclude that there exists an impact energy threshold below which damage cannot be found (~2 Joules for the present material system and lay-up).

Other researchers have also reported the existence of a threshold energy for impact damage. Choi et al. [36] reported a threshold impact energy for T300/976 graphite epoxy cross-ply composites and also indicated a stacking sequence effect on the threshold value. Reported values range from 0.52 to 3.1 J. The value here is somewhat low which may be related to the very small impact window. This will be investigated in the future. Strait et al. [37] studied IM7/977-2 thermoplastic laminates with various lay-ups, including cross-ply and quasi-isotropic. The normalized energy per unit thickness at the onset of incipient damage was found to be approximately 1.5 J/mm (or 9.75 Joules, if expressed in the total impact energy). These values are much higher than observed in the present investigation, indicating the influence of toughened epoxy systems on impact damage size.

5.2 COMPRESSIVE STRENGTH AFTER IMPACT (CSAI).

Compressive strengths and delamination size at different incident impact energy levels (E_i) are shown in figure 5 and table 3. The reduction in compressive strength closely follows the increase in delamination diameter. The average CSAI (600 MPa) of specimens without damage is comparable to that of unimpacted specimens (UCS = 621 MPa). Increasing impact energy slightly above the impact threshold level results in a CSAI of 470 MPa, a 25% reduction from the unimpacted strength. Since the objective of this research is to investigate the fatigue growth of barely visible impact damage, an incident impact energy of 2.1 J producing a repeatable delamination of ~12.7 mm was chosen for subsequent fatigue studies.

Stellbrink [12] reported a CSAI reduction of ~50% for T300/69 and T300/914 quasi-isotropic laminates with d/w (delamination diameter to specimen width) ratios of 0.32-0.44, while Ramkumar [13] observed ~65% reduction for AS4/3501-6 laminates. Although the d/w in Ramkumar's study is almost the same as in the current study (i.e., d/w of 0.33), strength reductions are substantially different. The actual delamination failure of the specimens in the present study occurred at ~430 MPa (figure 6), while the final collapse occurred later at ~470 MPa (i.e., CSAI). The delamination failure is defined as the separation of the thin surface layer on the rear side of impact, and it is usually accompanied by a large popping sound. That is,

the delaminated ply or plies first buckle locally at between 80% and 90% of the CSAI causing delamination growth first towards the sides and then axially leading to the failure of the whole laminate (figure 6).

5.3 POST-IMPACT FATIGUE BEHAVIOR.

A total of 68 impacted specimens were tested in fatigue under various loading conditions as indicated in tables 4, 5, and 7 (2 to 3 specimens were tested under each loading condition).

5.3.1 Constant-Amplitude Tension-Tension Loading.

A total of four 24-ply specimens were tested under constant-amplitude T-T loading at load levels of 50% and 60% of the ultimate tensile strength (UTS) of the undamaged specimens (table 4). The influence of two initial impact energies on subsequent tension-dominated fatigue was investigated: the same absolute initial impact energy (~2 J) that was used in the case of compression-dominated loading of thicker 32-ply specimens and the same energy normalized per unit thickness (0.5 J/mm) used for 32-ply specimens which resulted in the lower initial impact energy (1.5 J). This resulted in two slightly different initial damage parameters which are outlined in table 4 and figure 7. However, in both cases impact damage growth was not observed under subsequent tension-dominated fatigue (see figure 7). As in the case of the undamaged specimens edge delamination and ply cracking were the predominant damage modes for these coupons. This agrees well with the results of other researchers (Ramkumar [13]) who indicated that tensile loading, static or fatigue, represents the least threat to impact damaged laminates. However, greater impact energy and/or larger specimens need to be tested to fully investigate the effect of impact damage growth under tensile loading.

5.3.2 Constant-Amplitude Tension-Compression Loading.

As in the case of T-T fatigue, the damage growth under T-C fatigue resembled that of unimpacted specimens. Specimens cycled at ±30% CSAI showed only ply cracking, with an absence of delamination growth up to 10^6 cycles. At higher load levels of ±40% and ±50% CSAI, both ply cracking and edge delamination were observed together with a minor growth of initial damage. Radiographs showing typical damage growth pattern in coupons tested at ±50% CSAI are presented in figure 8. While a very thin delaminated region grew from the impact-induced delamination, edge delaminations actually governed the fatigue life, similar to unimpacted specimens. That is, a comparison of T-C *S-N* curves between impacted and unimpacted specimens (Hahn et al. [2]) revealed little differences between the two (figure 11(a)). Due to the severity of T-C loading, failure of these laminates occurred at lower load levels than in constant-amplitude C-C.

5.3.3 Constant-Amplitude Compression-Compression Loading.

The extent and mode of delamination growth under C-C fatigue varied significantly depending on the applied load level. For specimens cycled at 40% and 50% CSAI, the impact-induced damage did not grow under cyclic loading up to 10^6 cycles. Furthermore, residual compression tests of these specimens indicated that the post-fatigue compressive strength was not influenced

by these low loads (see RCS results in table 4). At 60% CSAI, impact damage grew slightly in one specimen up to 10^6 cycles (see figure 9). At higher load levels, 70% and 80% CSAI, more severe damage growth was observed, as shown in figure 10. Although there were some variations between specimens cycled at 70% CSAI, delamination extended throughout the entire gage section at ~10,000 cycles. Delamination growth at this load level initiated after ~100 cycles and occurred at a depth of one or two plies from the rear side of impact. Subsequent buckling of these plies was the major driving force for delamination propagation. Another important characteristic of the impact damage growth is that delamination propagated only on the rear side of the specimen making its detection from the impact side very difficult.

Examination of damage growth patterns in figure 10 reveals that initial separation of the thin layer from the base sublaminate (damage initiation) was more extensive in the width direction. However, subsequent propagation of delamination in fatigue was oriented more towards the tab region, along the loading direction. Other researchers (Blaricum et al. [15] and Ramkumar [13]) suggest that the damage width is the major factor governing fatigue delamination growth in impacted specimens. While different material systems were investigated in these two studies, laminate stacking sequences were similar, with the same outer ply configuration [+45/-45/0/0...]$_S$. In another study (Ramkumar [14]), delamination growth and its direction was shown to be dependent on the laminate stacking sequence and its through-the-thickness location. For laminates with the outer 0° ply, fatigue failure was induced predominantly by the propagation of delamination to the tab region (in the loading direction), similar to the observations in the current study.

In this study, the delamination length in the loading direction was selected as a damage growth parameter, rather than the damage width or area. However, it should be pointed out that this is merely a consequence of the laminate stacking sequence and the location of damage through-the-thickness (as investigated in this study), and it does not represent a unique delamination growth parameter. Delamination length as a function of number of fatigue cycles is shown in figure 12 for two load levels, 70% and 80% CSAI (average of three specimens). The best-fit function of the experimental data presented in this figure (solid lines) is assumed to be of the form:

$$L = a + bN^c \qquad (3)$$

where L is the delamination length [mm], N is the number of cycles, and a, b, and c are best-fit parameters (see table 6). As shown in figure 12 delamination extended the entire gage length at ~700 cycles at 80% CSAI and ~10,000 cycles at 70% CSAI. Since negligible delamination growth was observed for load levels below 70%, these results suggest that 70% CSAI represents a threshold value to initiate delamination growth of barely visible impact damage.

A comparison of C-C S-N curves of impacted and unimpacted specimens (Hahn et al. [2]) is presented in figure 11(b). Stress levels in this figure were normalized by the ultimate compressive strength (UCS) of unimpacted specimens (100% CSAI corresponds to 75% UCS). While the final failure of the specimens tested at 80% CSAI closely followed observed damage growth, catastrophic failure of specimens tested at 70% CSAI occurred much later, at more than 100,000 cycles (see table 4). However, it is evident that the fatigue life of impacted specimens

10

was reduced when compared to unimpacted coupons, especially at higher load levels (> 60% CSAI) where delamination growth governed the fatigue response. At lower load levels for which damage did not grow, similar performance in terms of life was observed.

5.3.4 Compression-Compression Fatigue: Two-Level Block Loading.

In order to determine the fatigue limits for impacted composite laminates, constant-amplitude tests can provide useful information about the damage growth and fatigue life at different load levels. Based on the results of constant-amplitude fatigue and residual compression tests, the fatigue limit was found to be 60% CSAI in C-C fatigue and ±30% CSAI in T-C fatigue. However, it has been suggested that delamination in composite materials may grow very rapidly for a small load range and that small uncertainties in the applied load may lead to large uncertainties in delamination growth (O'Brien [19]). This is especially important if the service loads are greater than anticipated. Therefore, the influence of high load levels (70% CSAI) was investigated next, since only minor damage growth was observed for specimens tested at 60% CSAI.

5.3.4.1 Low/High Block-Loading Sequence.

Two specimens were subjected to low/high block loading to assess the influence of this load sequence on damage propagation. After one million cycles at 40% CSAI without visible damage growth, fatigue was continued at 70% CSAI until final failure (40/70). Delamination growth (figure 13) and number of cycles at 70% CSAI to final failure (table 5) were very similar to the coupons that were tested only at 70% CSAI. For other fatigue damage modes in composite materials, two-level block-loading tests have shown that low/high load sequence results in a greater damage than high/low test sequence. Examples include ply cracking in T-T fatigue (Hahn et al. [2]) and splitting around the hole in notched composite laminates (Choi et al. [38]). For those cases, the low loads by themselves may not be damaging but they may enhance damage growth at high load levels (ply cracking), or on the other hand, high loads might retard damage growth in low amplitude fatigue (splitting). For the type of damage investigated in this study the exact opposite behavior was observed since low loads did not contribute to accelerated delamination growth at higher load amplitudes. However, it should be pointed out that different load magnitudes as well as the number of cycles in each block could change aforementioned observations. For example, load sequences of 50/30 and 30/50 would not show any differences between the two since constant-amplitude fatigue at both 30% and 50% CSAI did not lead to damage growth or fatigue failure.

5.3.4.2 High/Low Block-Loading Sequence.

Twenty specimens were tested in a high/low block-loading sequence. The first block (high) was the same for all specimens while the loading parameters of the second block (low) were varied. The first block consisted of 100 cycles at 70% CSAI (R = ∞) and is denoted in the remainder of this document as the *preload*. This specific number of cycles at this load level was chosen to initiate damage growth and to obtain a repeatable damage pattern before the beginning of the second block. Loading parameters of the second block are shown in table 5 and figure 17, and they are summarized below:

11

- Constant maximum load, variable load range
    - S_{max} = constant = 0% CSAI
    - ΔS = 30, 40, 50, 60% CSAI

- Constant minimum load, variable load range
    - S_{min} = constant = 60% CSAI
    - ΔS = 20, 30, 40, 60% CSAI

- Constant load range, variable minimum load
    - ΔS = constant = 30% CSAI
    - S_{min} = 30, 40, 50, 60, 70% CSAI

The second block was terminated after one million cycles or after delamination reached the tab region of the specimen, whichever occurred first. Loading parameters of the second block were chosen so that results of these tests could be used to analyze or predict damage growth in spectrum fatigue via a cumulative damage model. The loading conditions of the TWIST spectrum are explained in the next section and in table 8.

A typical damage growth for high/low block loading are shown in figures 14-16, while the summary of delamination growth as a function of fatigue cycles is presented in figures 18 and 19 for all high/low load sequences. As indicated in these figures, following the overloads that initiated damage growth (100 cycles at 70% CSAI), delamination propagated even at load levels for which damage did not grow in constant-amplitude fatigue. Cyclic growth rates (dL/dN in mm/cycle) as a function of delamination length (L) are also shown in figure 19. This figure indicates that delamination cyclic growth rates decreased with an increase in delamination size, the effect being more pronounced for lower load ranges. While both the load range (ΔS) and the maximum compressive stress (S_{min}) influence delamination growth, it is evident that ΔS has a slightly larger influence on damage growth. A summary of these results, as a function of the mean stress and stress amplitude ($S_a = 1/2 \Delta S$), is presented in constant life diagram in figure 20. Note that the N indicated in this figure does not represent number of cycles to failure, but indicates the number of cycles that caused propagation of delamination to the tab region. As can be seen from this figure, as long as the load range (ΔS) is equal to or less than 20% of CSAI, delamination growth is not significant.

Similar decreases in cyclic growth rate have been reported by other researchers (Whitcomb [39-40]) who investigated the growth of a single delamination under compression loading and suggested that delamination may arrest without degrading the performance of composite laminates. While complex damage consisting of multiple delaminations was investigated in the current study, damage growth characteristics were very similar to the studies performed on single implanted delaminations (Whitcomb [39-40]). That is, after the separation of the thin surface layer from the base laminate, the subsequent behavior under fatigue loading resembled the single delamination growth.

These results indicate the deleterious effect of high load excursions on damage growth. Once delamination growth was initiated (separation of the thin surface layer from the base laminate),

the forces required to propagate delamination were substantially smaller than the forces required to initiate delamination growth. Fatigue design in the presence of barely visible impact damage (BVID) should focus on determination of the high load levels that initiate damage growth, since following these overloads, the delamination propagation threshold is ~30% CSAI. That is, for ΔS less than 30% CSAI, delamination growth rates were not significant and they approached 10^{-6} mm/cycle.

5.3.5 Compression-Dominated Blocked TWIST Loading.

The results of the constant-amplitude C-C tests indicated that impact-induced damage did not grow when the highest load levels were below the levels that initiate delamination growth (70% CSAI). Since high load levels represent less than 0.05% of the total number of cycles in the transport wing spectrum test (realistic service conditions), their magnitude and sequence of occurrence is very important for appropriate durability design. Furthermore, results of two-level block-loading tests indicated that the high/low loading sequence induced more damage than the low/high test sequence. Although this behavior could influence damage propagation within the first block of blocked TWIST spectrum, after 10 repetitions of each block (total of 40,000 flight hours) the differences should not be significant. Another important parameter of the spectrum fatigue is the flight mean load (FML) since it determines the 10 load excursion levels. Three different FMLs were investigated in this study: 25%, 27.5%, and 30% CSAI. The maximum compressive loads for these three test conditions were 65%, 72%, and 78% CSAI respectively as outlined in table 7. These were chosen to obtain damage growth. It should be noted that although the spectrum load was compression dominated, some load excursions were high enough to produce tension loads up to +18% CSAI.

A total of 18 specimens were tested under the blocked TWIST spectrum as indicated in table 8. Nine specimens were evaluated under the full-spectrum loading, while nine specimens were tested with the two lowest load levels deleted from the test sequence (modified spectrum). In both the full and modified test spectrums, the impact damage growth during fatigue loading was observed in samples tested at mean load levels of 27.5% and 30% CSAI. Specimens tested at FML = 25% CSAI, with the maximum compressive load of 65% CSAI, did not exhibit any damage growth during these tests.

5.3.5.1 FML = 27.5% CSAI.

Three specimens were tested using the full spectrum and three using the modified spectrum at 27.5% CSAI flight mean and all of them survived 10 blocks. While in some specimens, delaminations started to grow after the first block of TWIST spectrum, the others did not display any damage growth up to 10 blocks. Although 10 blocks of TWIST loading consisted of ~4 million cycles at various load levels, at 27.5% flight mean level only 30 cycles were at, or above, 70% CSAI. In constant-amplitude C-C loading at this load level (70%) the number of cycles to initiate delamination growth was between 1 and 100 cycles. Therefore, large variations in the damage growth under spectrum conditions is acceptable when the variability observed under constant-amplitude loading is taken into account. Comparison between damage patterns in coupons tested using the full and modified spectrum did not reveal significant differences between the two. Furthermore, in the full-spectrum loading the damage did not grow at low-load

levels. To illustrate this point, damage growth in one specimen as a function of completed load levels within the first block of loading and as a function of completed blocks is presented in figure 21. As shown in this figure, appreciable damage growth occurred after completing the first two load levels (a total of three cycles at the two highest levels). However, damage did not change significantly after fatigue at lower load levels (393,465 cycles at the two lowest levels). A similar pattern was observed within the other blocks for this same coupon and for other specimens in this study. That is, damage growth was only due to the high-load excursions, while delamination propagation was negligible at low-load levels (ΔS = 12-20% CSAI). Final damage patterns after 10 blocks of TWIST loading are shown in figure 22 for all specimens tested under 27.5% flight mean load.

5.3.5.2 FML = 30% CSAI.

Three specimens were tested using the full spectrum at 30% mean load: two survived 10 blocks while one failed after completing 7 blocks, that is, during the first cycle of the highest load level of block 8. Damage growth was observed in both the full and modified spectrum (figure 23), however, no failure was observed in three specimens tested in modified spectrum. Comparison between delamination growth in full and modified spectrum at FML = 30% CSAI is presented in figure 24. The solid line in this figure represents delamination growth prediction of the linear cumulative damage model based on the history-independent damage growth (Hwang and Han [41]). Cyclic growth rates generated during the constant-amplitude and two-level block loading (see figures 18 and 19) were used to predict damage development during spectrum loading. The influence of the two lowest load levels was neglected in constructing this diagram such that the damage prediction presented in figure 24 applies both to full and modified spectrum. Cyclic range ($\Delta S = S_{max} - S_{min}$) of the two lowest load levels for these cases were 13% and 22% CSAI (see table 7) for which, according to results of constant-amplitude fatigue, cyclic growth rates approach 10^{-6} mm/cycle leading to a negligible effect on overall damage growth. Although there is similarity between the model prediction and experimental data (figure 24), large scatter in damage patterns makes it difficult to reach a definitive conclusion about the model's predictive capabilities and regarding the influence of spectrum modification on damage propagation. However, as mentioned earlier in this section, monitored damage growth within the full spectrum (figure 21) clearly delineates the influence of certain load levels on damage growth, suggesting that the two lowest load levels (which represent 98.69% of the whole spectrum) can be deleted from the test sequence without significant influence on impact damage propagation.

5.4 RESIDUAL COMPRESSIVE STRENGTH EVALUATION.

To determine the influence of fatigue cycling on residual strength, 31 specimens were tested in static compression according to the procedure outlined in section 3.2 (figure 2). That is, after completing fatigue loading the specimens were cut into smaller coupons and the residual compressive strength (RCS) was determined. The summary of these results is outlined in tables 4, 5, and 8 and it is graphically represented in figure 25. Also included in this figure are radiographs of two specimens indicating the final damage after fatigue. As shown in this figure, compressive strength after fatigue did not change with respect to the initial strength reduction (due to impact) even for the coupons in which the delamination extended the entire gage length.

14

Average value for RCS was 483 MPa which was slightly higher than the average compressive strength of impacted samples (CSAI = 470 MPa). These results suggest that the residual strength was not sensitive to additional fatigue damage (i.e., delaminations that span only a few surface plies). This is in agreement with the results of other researchers who suggested that although compression strength is greatly influenced by the impact damage, any subsequent reduction under fatigue loading is minimal (O'Brien [19]).

Comparisons between the results presented in figure 25 and figure 5(b) indicate that although the overall damage area was larger for fatigued samples (figure 25) than for the specimens impacted with high energy (figure 5(b)), strength reduction in fatigued samples was much smaller. That is, the extension of damage through the thickness of the laminate together with the overall damaged area could provide better representation of impact and fatigue damage and its influence on compressive strength reduction. The overall delamination area (or length) does not represent a reliable damage parameter for residual strength.

5.5 RESULTS OF ANALYTICAL STUDIES.

Experimental results indicate that once the damage propagated it resembled a single delamination growth located one or two plies below the laminate surface. To gain a physical understanding of the mechanisms contributing to the delamination propagation, the correlation between the cyclic growth rates and the strain energy release rates (G) was investigated. Buckling and postbuckling response of a thin portion of the laminate was modeled as described in section 4 using the model. G_I and G_{II} values of figures 26 and 27 were calculated at different strain levels for delaminations located at one ply and two plies beneath the surface, respectively. It should be noted that from the experimental stress-strain curves of impacted samples, 100% CSAI roughly corresponds to 1.15% far-field strain.

In figure 26 only values calculated for the mode II component (G_{II}) are shown since values for G_I are essentially zero. That is, in the case of a single ply, G_I values are very small due to the low bending stiffness of the delaminated ply. As the thickness of the delaminated ply increases, G_I also increases (Whitcomb [39]). This is shown in figure 27 for the case when the delamination is located two plies beneath the laminate surface. Note that the values for G_{II} have increased only slightly when compared to the G_{II} for the deep delamination one-ply solution (figure 26) while there is a substantial increase in the mode I component. However, the influence of mode I on damage growth decreases rapidly as the crack length increases, and it would not contribute to the delamination growth once the delamination reaches ~18 mm. On the other hand, values of G_{II} remain relatively constant over the range of delamination lengths investigated; therefore, a constant value of G_{II} can be assumed for a specific value of applied strain. However, after the initial buckling of the delaminated plies, the crack tip actually closes due to the compressive forces that develop near the crack tip. (For a detailed discussion on the mechanics of instability related delamination growth, the reader is referred to papers by Whitcomb [20-22,39-40].) These compressive forces might decrease the calculated values for G_{II}, thus leading to the decay of cyclic growth rate.

The fatigue-induced delamination growth rate criterion, which separates the contribution of mode I and mode II, is usually assumed to be of the form (Ramkumar and Whitcomb [42]):

$$\frac{dL}{dN} = m_1 \left(\frac{G_I}{G_{Ic}}\right)^{n_1} + m_2 \left(\frac{G_{II}}{G_{IIc}}\right)^{n_2} \tag{4}$$

where dL/dN is the cyclic growth rate in mm/cycle, m_1, m_2, n_1, and n_2 are experimentally determined constants. Critical values of strain energy release rates, as determined by other researchers (G_{Ic} and G_{IIc}) for this material system, are listed in table 9. The average value for G_{IIc} = 532 N/m from this table is used in subsequent calculations. It should also be noted that values listed in table 9 are under static load. Under cyclic load, lower critical strain energy values have been measured. Based on the previous arguments (see figures 26 and 27), a delamination growth criteria that incorporates only mode II components were investigated ($dL/dN = f(G_{II})$).

For fatigue tests performed at R = ∞, G_{II} is the same as G_{IImax} and ΔG_{II} (experimental data presented in figures 12 and 18(a)). Using these experimental values (equation 4) and calculated values for G_{II} in figure 27, constants m_2 and n_2 are determined to be 10 mm/cycle and 4.5, respectively. Comparison of associated cyclic growth rates as a function of delamination length with the best fit of experimental data is shown in figure 28. Good agreement for the cyclic growth rates is obtained for large delaminations (> 18 mm) but there is an apparent dissimilarity for smaller delamination lengths. Better correlation between experimental and analytical results would be obtained if the G_I values presented in figure 27 (two-ply buckling) were included since they are the dominant feature for L less than 18 mm. However, due to large differences between calculated G_I values for delamination spanning one and two plies, the influence of mode I on delamination growth was neglected in the current study.

For fatigue tests at different R ratios it is a common practice to determine different values for coefficients m_2 and n_2 by replacing G_{II} in equation 4 with the appropriate value of ΔG_{II}. In the present study, such a fit to the experimental data would lead to an increase in n_2 from 4.5 (R=∞) up to 8-10 for stress ratios between 2 and 4. The authors propose a different delamination growth rate criteria that includes the effects of both ΔG_{II} and G_{IImax}. The following expression was found to provide best fit of the experimental data for a wide range of stress ratios:

$$\frac{dL}{dN} = m_2 \left[\frac{\Delta G_{II}\left(\dfrac{\Delta G_{II}}{G_{max}}\right)}{G_{IIc}}\right]^{n_2} \tag{5}$$

This equation is similar to the approaches used to characterize crack growth rates in metals for different stress ratios (Broek [43]), and for R=∞ it reduces to equation 4 since $G_{IImax} = \Delta G_{II}$. A comparison of the analytical and experimental cyclic growth rates for three different R values is shown in figure 29. Again, good agreement in the cyclic growth rates is observed for larger delaminations for which mode II drives damage growth. Furthermore, an expression that incorporates both ΔG_{II} and G_{IImax} simplifies delamination growth characterization, since the same values for coefficients m_2 and n_2 were used in constructing cyclic growth curves in figures 28 and 29.

16

For a full understanding of parameters that influence delamination growth a complete three-dimensional finite element modeling is needed that includes the influence of laminate stacking sequence. However, a simplified modeling approach, as presented in this study, can still provide useful information about the major forces that drive delamination growth. For the type of damage growth investigated in this study (i.e., delamination that spans only a few surface plies) results suggest that mode II is the dominant factor that governs delamination growth with minor contributions from mode I for smaller delamination lengths. If the delamination is nested deep in the thickness of the laminate, the influence of mode I component becomes dominant and it can not be neglected (see figure 30). However, the maximum value of G_I occurs at different load levels for different delamination lengths and depths (Whitcomb [39]). Furthermore, large scatter in reported critical strain energy release rates (Shyprykevich [44] and table 9) and small uncertainties in loading spectrum and damage characteristics could lead to substantially different delamination growth predictions. Thus, it would be difficult to provide rationale for omitting certain load levels from the fatigue test sequence based on calculated delamination growth thresholds.

6. SUMMARY.

The long-term mechanical fatigue of quasi-isotropic graphite/epoxy laminates was investigated to determine the influence of loading parameters on impact-induced delamination growth during constant-amplitude and spectrum fatigue loading. Based on the test results, the following recommendations for fatigue design of composite laminates in the presence of barely visible impact damage (BVID) are suggested:

- In T-C fatigue-impacted and undamaged specimens show negligible difference in their *S-N* curves and damage growth modes, as the predominant damage mode is tension dominated edge delamination and not impact caused delamination. Greater impact energy and larger specimens need to be tested to investigate the effect of impact damage growth under tensile loading.

- A fatigue limit of 60% CSAI is recommended in constant-amplitude C-C fatigue and 65% CSAI in compression-dominated spectrum loading, as represented by TWIST.

- Compression fatigue at high stress levels (70% and 80% CSAI) leads to extensive growth of impact-induced delamination and the fatigue life is significantly reduced.

- Following overloads (high load excursions greater than 70% CSAI) which initiate delamination growth, a delamination propagates in C-C fatigue due to local buckling even when the minimum compressive stress is reduced to 30% CSAI (i.e., high/low loading sequence). This leads to the conclusion that two-level C-C block-loading tests are more damaging than the low/high sequence.

- The cyclic growth rate of impact-induced delamination decreases with increasing delamination size. It appears that the mode II strain energy release rate governs the high delamination growth rates at large compressive fatigue stresses and for longer

17

delaminations, while the sharply reduced delamination growth rates at lower stress levels (shorter delaminations) are attributed to the mode I component.

- In compression-dominated spectrum fatigue the two lowest load levels (which represent 98.69% of the whole spectrum) can be deleted from the test sequence without significant influence on impact damage propagation and fatigue life. That is, durability testing can be accelerated by omitting those cycles whose load range (ΔS) is equal to or less than 20% CSAI.

- Residual compressive strengths of specimens subjected to compression-dominated fatigue are not sensitive to the subcritical damage which forms during fatigue (i.e., delaminations that span only a few surface plies).

- The overall delamination area (or length) alone does not represent a reliable damage parameter for residual strength. The extent of damage through the thickness of the laminate together with the overall damage area provides a better representation of impact damage and its influence on compressive strength.

Based on these results it is suggested that a conservative (no damage growth) damage tolerance criteria in the presence of BVID can be based on static tests and a limited number of constant-amplitude fatigue tests to determine (and avoid) the load levels that initiate delamination growth. For the type of impact damage and laminate configuration investigated in this study the maximum compressive strain should be kept below 0.69% (60% CSAI) in constant-amplitude loading and 0.75% (65% CSAI) under spectrum loading. In constructing a test spectrum to ascertain impact damage growth, all cycles equal or higher than 60% CSAI and with a range (ΔS) equal or greater than 20% CSAI must be part of the testing protocol. It is also recommended that loading blocks should be sufficiently small to avoid high-low or low-high load effects.

7. FUTURE WORK.

The future study will primarily focus on the effect of spectrum loading on the damage growth in notched and impacted specimens. It should be noted that the results reported in this report on impact-damaged composite laminates apply to the specimens impacted with an impact energy close to the delamination threshold energy. Also, maximum stress that these laminates can sustain without failure and growth of delamination (for compression-compression fatigue) is ~60% of CSAI, which roughly corresponds to 0.69% strain. This value is higher than the strain range that the actual aircraft structure experiences in service and may give unreasonably long estimates of fatigue life. To gain further insight into the effect of load parameters on impact damage propagation, higher impact energy and geometric parameters will be investigated in the upcoming period. Studying initial damage patterns different than the one employed in the current study (larger initial delamination area) is important if the certification procedures are to be developed based on the load levels associated with CSAI. Results from previous studies indicate high dependence of damage growth parameters for different damage and specimen sizes. Therefore, extrapolation of results corresponding to different geometry effects is not well understood and requires further investigation to determine the laws of scaling and how they

affect fatigue design of composite materials. Once these parameters are determined, a broad certification procedure covering a wide range of impact and geometric parameters can be established.

The experimental test matrix for this project is presented in tables 10 and 11, indicating the type of loading, modification of the spectrum, and number of specimens that will be tested at each load type. Note that proposed tests for impacted specimens are similar to the ones employed in the current study so that the direct comparison with different impact energy and specimen sizes can be made. Tension- and compression-dominated spectrum loading of notched specimens will also be performed as well as a number of constant-amplitude fatigue tests. The future part of this research is divided into three task areas.

7.1 TASK 1. IMPACT DAMAGE CHARACTERIZATION AND FATIGUE LOADING.

Initial impact testing will be performed to determine the relationship between the impact energy, induced damage, and compressive strength after impact. Based on the results of static compression tests and constant-amplitude fatigue, the spectrum flight mean load and alternating load levels will be determined. Monitoring damage progression during fatigue loading will be done periodically to assess the change of the damaged area as a function of loading parameters. Full TWIST tests will be performed at only one flight mean load level to determine the influence of all load levels on damage growth. This will be compared to the results of a modified spectrum in which the influence of deletion will be studied through the omission of the two lowest levels (0.222 and 0.375). The objective of this part is to shorten testing time but retain the damage developed with full-spectrum testing. The lowest load levels are the largest portion of the TWIST spectrum (in terms of testing time), since they represent more than 98% of the whole spectrum. Deletion of other load levels would not contribute to test time savings, as could the two lowest load levels. Both tension- and compression-dominated spectrum behavior will be studied, and the total number of specimens tested during this part of the project will be 45. Selected specimens from each of the tests will be tested for residual strength characterization. Following the fatigue testing, some of the specimens will be sectioned and inspected microscopically to assess the extent of damage accumulated during fatigue loading on a ply-by-ply basis.

7.2 TASK 2. NOTCHED STRENGTH CHARACTERIZATION AND FATIGUE LOADING.

The proposed test matrix for notched (open-hole) coupons is presented in table 11. Based on the results of constant-amplitude tests, the spectrum flight mean load and alternating load levels will be determined. Monitoring damage progression in the form of matrix cracking, delamination, and splitting during fatigue loading will be done periodically to assess this type of damage growth as a function of loading parameters. Full TWIST tests at 10 Hz will be done to obtain baseline data, and these will be compared to the modified spectrums (table 11) that are already outlined in Task 1 for impacted specimens. Again, the objective of these modifications is to develop procedures which will shorten testing time but retain the damage developed within the full-spectrum test.

8. REFERENCES.

1. Hahn, H.T., J. Timmer, J. Bartley-Cho, and S.G. Lim, "The Effect of Preloading on Fatigue Damage in Composite Structures: Part 1," *DOT/FAA/AR-95/79*, April 1996.

2. Hahn, H.T., J. Bartley-Cho, and S.G. Lim, "The Effect of Loading Parameters on Fatigue of Composite Laminates: Part II," *DOT/FAA/AR-96/76*, July 1997.

3. Lammerant, L. and I. Verpoest, "The Interaction Between Matrix Cracks and Delaminations During Quasi-Static Impact of Composites," *Composite Science and Technology*, **51**, 1994, pp. 505-516.

4. Choi, H.Y. and F.-K. Chang, "A Model for Predicting Damage in Graphite/Epoxy Laminated Composites Resulting from Low-Velocity Point Impact," *Journal of Composite Materials*, **26** (14), 1992, pp. 2134-2169.

5. Baker, A.A., R. Jones, and R.J. Callinan, "Damage Tolerance of Graphite/Epoxy Composites," *Composite Structures*, **4**, 1985, pp. 15-44.

6. Clark, G. and T.J. van Blaricum, "Load Spectrum Modification Effects on Fatigue of Impact Damaged Carbon Fibre Composite Coupons," *Composites*, **18** (3), July 1987, pp. 243-251.

7. Clark, G. and D.S. Saunders., "Morphology of Impact Damage Growth by Fatigue in Carbon Fibre Composite Laminates," *Materials Forum*, **15** (1), 1991, pp. 333-342.

8. Konishi, D.Y. and W.R. Johnston, "Fatigue Effects on Delaminations and Strength Degradation in Graphite/Epoxy Laminates," *Composite Materials: Testing and Design (Fifth Conference), ASTM STP 674*, S.W. Tsai, Ed., ASTM, 1979, pp. 597-619.

9. Ong, C.L., M.F. Sheu, Y.Y. Liou, and T.J. Hsiao, "The Study of the Fatigue Characteristics of Composite After Impact," *36th International SAMPE Symposium*, Vol. 1, April 1991, pp. 912-923.

10. Portanova, M.A., C.C. Poe, and J.D. Whitcomb, "Open Hole and Postimpact Compressive Fatigue of Stitched and Unstitched Carbon-Epoxy Composites," *Composite Materials: Testing and Design (Tenth Volume), ASTM STP 1120*, G.C. Grimes, Ed., ASTM, 1992, pp. 37-53.

11. Saunders, D.S. and T.J. van Blaricum, "Effect of Load Duration on the Fatigue Behavior of Graphite/Epoxy Laminates Containing Delaminations," *Composites*, **19** (3), May 1988, pp. 217-228.

12. Stellbrink, K.K.U., "Influence of Low-Velocity Impact on the Fatigue Behavior of CFRP Laminates," *Fatigue and Creep of Composite Materials, Third International Symposium on Metallurgy and Material Science*, 1982, pp. 319-327.

13. Ramkumar, R.L., "Effect of Low-Velocity Impact Damage on the Fatigue Behavior of Graphite/Epoxy Laminates," *Long-Term Behavior of Composites, ASTM STP 813*, T.K. O'Brien, Ed., American Society for Testing and Materials, Philadelphia, 1983, pp. 116-135.

14. Ramkumar, R.L., "Compression Fatigue Behavior of Composites in the Presence of Delaminations," *Damage in Composite Materials, ASTM STP 775*, K.L. Reifsnider, Ed., American Society for Testing and Materials, 1982, pp. 184-210.

15. van Blaricum, T.J., D.S. Saunders, G. Clark, and T.E. Preuss, "Damage Tolerance of Impact Damaged Carbon Fibre Composite Wing Skin Laminates," *New Materials and Fatigue Resistant Aircraft Design, 14th Symposium of the Int. Committee on Aeronautical Fatigue*, Edited by D.L. Simpson, 1987, pp. 537-556.

16. Cairns, D.S. and P.A. Lagace, "Residual Tensile Strength of Graphite/Epoxy and Kevlar/Epoxy Laminates with Impact Damage," *Composite Materials: Testing and Design (Ninth Volume), ASTM STP 1059*, S.P. Garbo, Ed., ASTM, Philadelphia, 1990, pp. 48-63.

17. Ratwani, M.M. and H.P. Kan, "Effect of Stacking Sequence on Damage Propagation and Failure Modes in Composite Laminates," *Damage in Composite Materials, ASTM STP 775*, K.L. Reifsnider, Ed., American Society for Testing and Mat., 1982, pp. 211-228.

18. Demuts, E., R.S. Whitehead, and R.B. Deo, "Assessment of Damage Tolerance in Composites," *Composite Structures*, Vol. 4, 1985, pp. 45-58.

19. O'Brien, T.K., "Towards a Damage Tolerance Philosophy for Composite Materials and Structures," *Composite Materials: Testing and Design (Ninth Volume), ASTM STP 1059*, S.P. Garbo, Ed., ASTM, Philadelphia, 1990, pp. 7-33.

20. Whitcomb, J.D., "Three-Dimensional Analysis of a Postbuckled Embedded Delamination," *Journal of Composite Materials*, 23, 1989, pp. 863-889.

21. Whitcomb, J.D., "Mechanics of Instability-Related Delamination Growth," *Composite Materials: Testing and Design (Ninth Volume), ASTM STP 1059*, S.P. Garbo, Ed., American Society for Testing and Materials, Philadelphia, 1990, pp. 215-230.

22. Whitcomb, J.D., "Analysis of a Laminate With a Postbuckled Embedded Delamination, Including Contact Effects," *Journal of Composite Materials*, 26 (10), 1992, pp. 1523-1535.

23. Kutlu, Z. and F.-K. Chang, "Modeling Compression Failure of Laminated Composites Containing Multiple Through-the-Width Delaminations," *Journal of Composite Materials*, **26** (3), 1992, pp. 350-387.

24. SACMA Recommended Test Method for Compression After Impact Properties of Oriented Fiber-Resin Composites, SRM 2-88.

25. General Research Corporation, "Model 8200 Drop Weight Impactor System," *Instruction Manual*.

26. ASTM Standard D 3410-87, "Standard Test Method for Compressive Properties of Unidirectional or Crossply Fiber-Resin Composites," *ASTM Standards and Literature References for Composite Materials*, 1989, pp. 131-140.

27. Phillips, E.P., "Effects of Truncation of a Predominantly Compression Load Spectrum on the Life of a Notched Graphite/Epoxy Laminate," *Fatigue of Fibrous Composite Materials, ASTM STP 723*, K.N. Lauraitis, Ed., ASTM, 1981, pp. 197-212.

28. Schütz, D., "Variable Amplitude Fatigue Testing," *Agard Lecture Series, AGARD-LS-118*, 1981, pp. 4/1 - 4/31.

29. Davidson, B.D., "Prediction of Delamination Growth in Laminated Structures," *Proceedings of the 1994 International Mechanical Engineering Congress and Exposition: Failure Mechanics in Advanced Polymeric Composites, AMD-Vol. 196*, Chicago, IL, USA, 1994, pp. 43-65.

30. Kardomateas, G.A., A.A. Pelegri, and B. Malik, "Growth of Internal Delaminations Under Cyclic Compression in Composite Plates," *Proceedings of the 1994 International Mechanical Engineering Congress and Exposition: Failure Mechanics in Advanced Polymeric Composites, AMD-Vol. 196*, Chicago, IL, USA, 1994, pp. 13-29.

31. Russell, A.J. and K.N. Street, "Predicting Interlaminar Crack Growth Rates in Compressively Loaded Laminates," *Composite Materials: Fatigue and Fracture (Second Volume), ASTM STP 1012*, P.A. Lagace, Ed., ASTM, Philadelphia, 1989, pp. 162-178.

32. Tratt, M.D., "Analysis of Delamination Growth in Compressively Loaded Composite Laminates," *Composite Materials: Fatigue and Fracture (Third Volume), ASTM STP 1110*, T.K. O'Brien, Ed., ASTM, Philadelphia, 1991, pp. 359-372.

33. Rybicki, E.F. and M.F. Kanninen, "A Finite Element Calculation of Stress Intensity Factors by a Modified Crack Closure Integral," *Engineering Fracture Mechanics*, 1977, Vol. 9, pp. 931-938.

34. Mukherjee, Y.X., S.N. Gulrajani, S. Mukherjee, and A.N. Netravali, "A Numerical and Experimental Study of Delaminated Layered Composites," *Journal of Composite Materials*, **28** (9), 1994, pp. 837-870.

35. Jih, C.J. and C.T. Sun, "Prediction of Delamination in Composite Laminates Subjected to Low Velocity Impact," *Journal of Composite Materials*, **27** (7), 1993, pp. 684-701.

36. Choi, H.Y., H.S. Wang, and F.-K. Chang, "Effect of Laminate Configuration and Impactor's Mass on the Initial Impact Damage of Graphite/Epoxy Composite Plates Due to Line-Loading Impact," *Journal of Composite Materials*, **26** (6), 1992, pp. 804-827.

37. Strait, L.H., M.L. Karasek, and M.F. Amateau, "Effects of Stacking Sequence on the Impact Resistance of Carbon Fiber Reinforced Thermoplastic Toughened Epoxy Laminates," *Journal of Composite Materials*, **26** (12), 1992, pp. 1725-1740.

38. Choi, S.W., M. Mitrovic, J.B.-Cho, H.T. Hahn, and P. Shyprykevich, "Effect of Loading Parameters on Fatigue Damage Development in Notched Composite Laminates," *43rd International SAMPE Symposium*, May 31-June 4, 1998, pp. 1257-1268.

39. Whitcomb, J.D., "Finite Element Analysis of Instability Related Delamination Growth," *Journal of Composite Materials*, **15**, 1981, pp. 403-426.

40. Whitcomb, J.D., "Strain-Energy Release Rate Analysis of Cyclic Delamination Growth in Compressively Loaded Laminates," *Effects of Defects in Composite Materials*, ASTM STP 836, ASTM, 1984, pp. 175-193.

41. Hwang, W. and K.S. Han, "Cumulative Damage Models and Multi-Stress Fatigue Life Prediction," *Journal of Composite Materials*, **20**, 1986, pp. 125-153.

42. Ramkumar, R.L. and J.D. Whitcomb, "Characterization of Mode I and Mixed-Mode Delamination Growth in T300/5208 Graphite/Epoxy," *Delamination and Debonding of Materials, ASTM STP 876*, W.S. Johnson, Ed., ASTM, Philadelphia, 1985, pp. 315-335.

43. Broek, D., *Elementary Engineering Fracture Mechanics*, M. Nijhoff Publishers, 1986.

44. Shyprykevich, P., "Damage Tolerance of Composite Aircraft Structures: Analysis and Certification," *Proceedings of ICCM-11*, Vol. I, Australia, July 1997, pp. 552-561.

45. Davies, P. and M.L. Benzeggagh, "Interlaminar Mode-I Fracture Testing," *Application of Fracture Mechanics to Composite Materials*, Edited by K. Friedrich, 1989, pp. 81-112.

46. Tian, Z. and S.R. Swanson, "Residual Tensile Strength Prediction on a Ply-by-Ply Basis for Laminates Containing Impact Damage," *Journal of Composite Materials*, **26** (8), 1992, pp. 1193-1206.
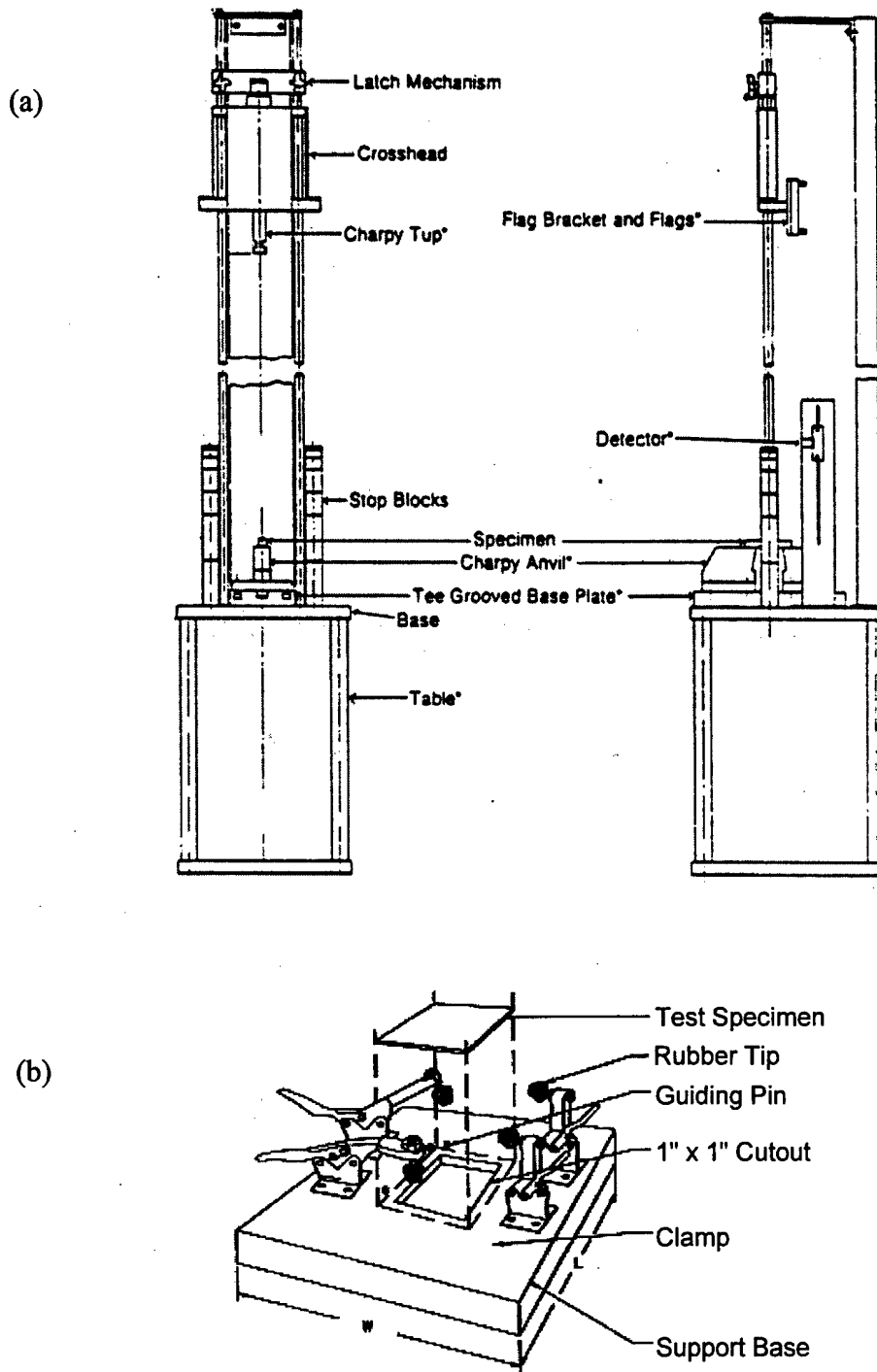
23

(a)

- Latch Mechanism
- Crosshead
- Charpy Tup*
- Flag Bracket and Flags*
- Detector*
- Stop Blocks
- Specimen
- Charpy Anvil*
- Tee Grooved Base Plate*
- Base
- Table*

(b)

- Test Specimen
- Rubber Tip
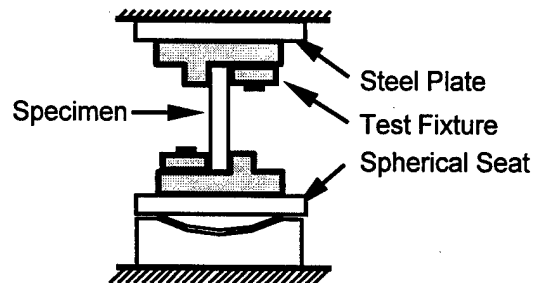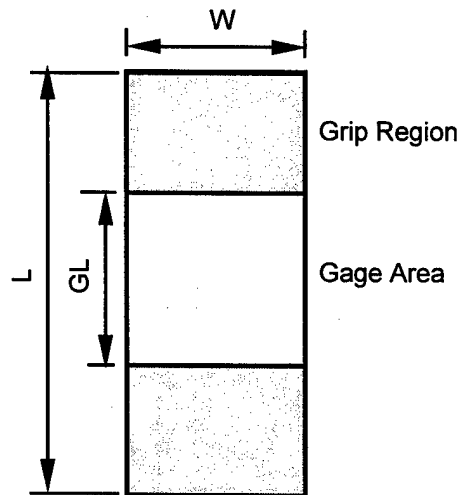- Guiding Pin
- 1" x 1" Cutout
- Clamp
- Support Base

FIGURE 1. IMPACT LOADING PARAMETERS (a) DYNATUP MODEL 8200 DROP
WEIGHT IMPACTOR [FROM 25] AND (b) MODIFIED SACMA SRM 2-88 IMPACT
FIXTURE [FROM 24]

24

Static Compression Evaluation

Modified NASA Short-Block
Compression Test Fixture

Specimen Dimensions

W = 38.1 mm
GL = 38.1 mm (T-C, C-C, and TWIST loading)
GL = 50.8 mm (static tension and T-T loading)
L = 57.1 mm (static compression testing)
L = 139.7 mm (T-C, C-C, and TWIST loading)
L = 152.4 mm (static tension and T-T loading)

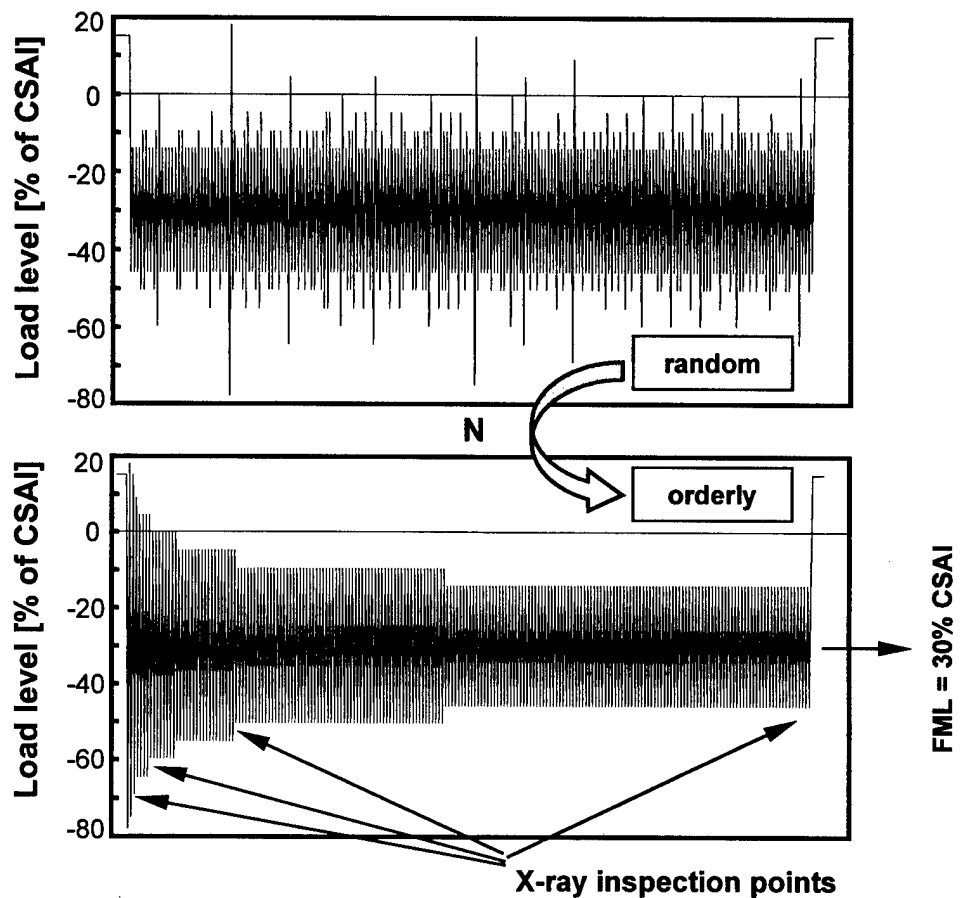FIGURE 2. STATIC COMPRESSION SETUP AND SPECIMEN DIMENSIONS

FIGURE 3. PROCEDURE FOR TWIST MODIFICATION: REDUCTION OF
COMPLETELY RANDOM OCCURRENCE OF LOAD LEVELS TO AN ORDERLY
SEQUENCE (FLIGHT A WITHOUT TWO LOWEST LOAD LEVELS,
FLIGHT MEAN LOAD = 30% CSAI)

Damage Growth Observed
Using X-Ray Radiography

Loading Direction

Plane Strain Finite Element Model:

u_x

Number of Elements: 60 x 14

a

w_{max}

Gap Elements Used Between
Two Delaminated Surfaces to
Prevent Overlap

Constrained in
y Direction

Constrained in
x Direction

y

x

Schematic of Finite Elements Near the Delamination Front (x-y Plane View)

a   b c_1

c_2

Δu_y

Crack Opening
Displacement
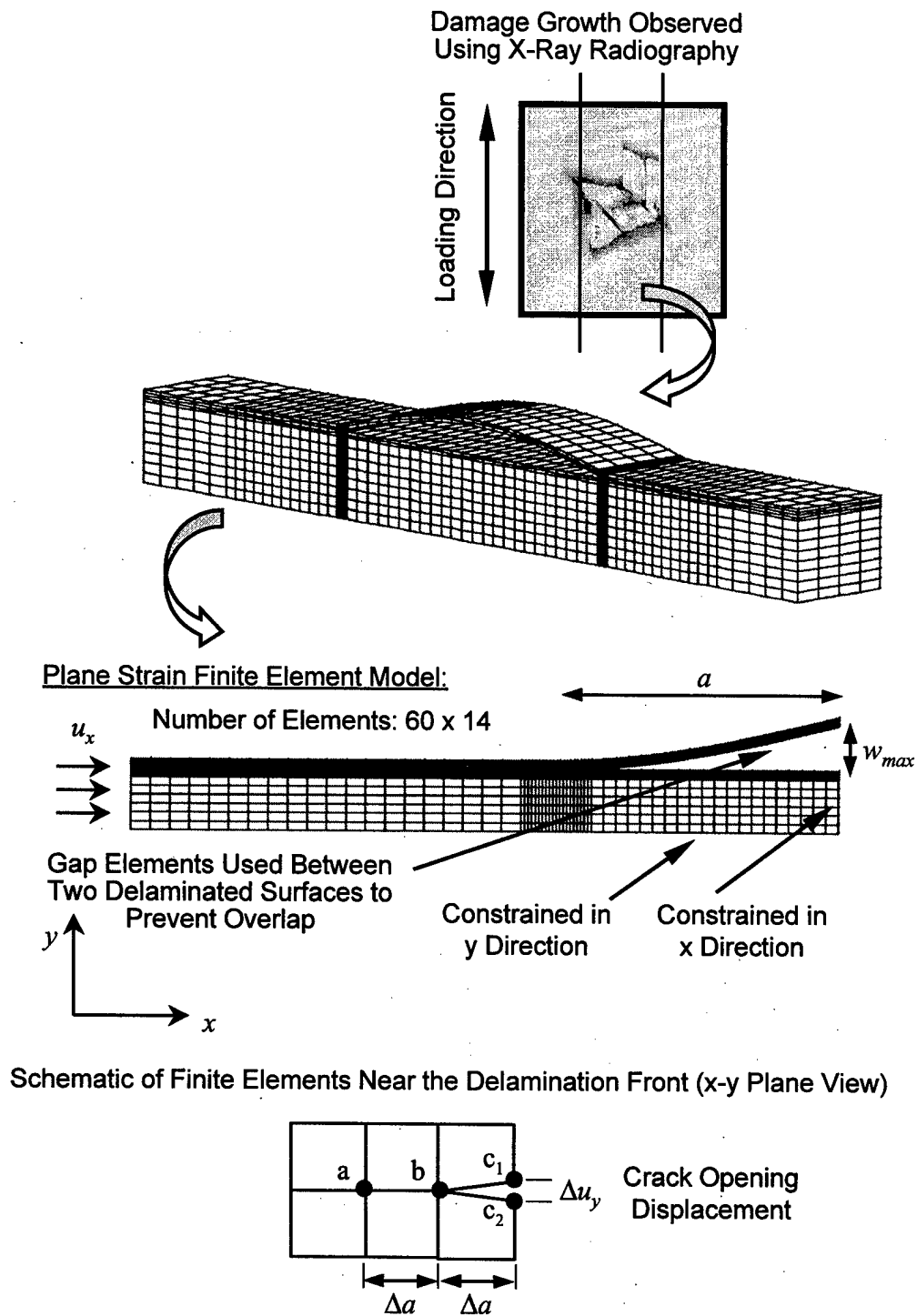
Δa Δa

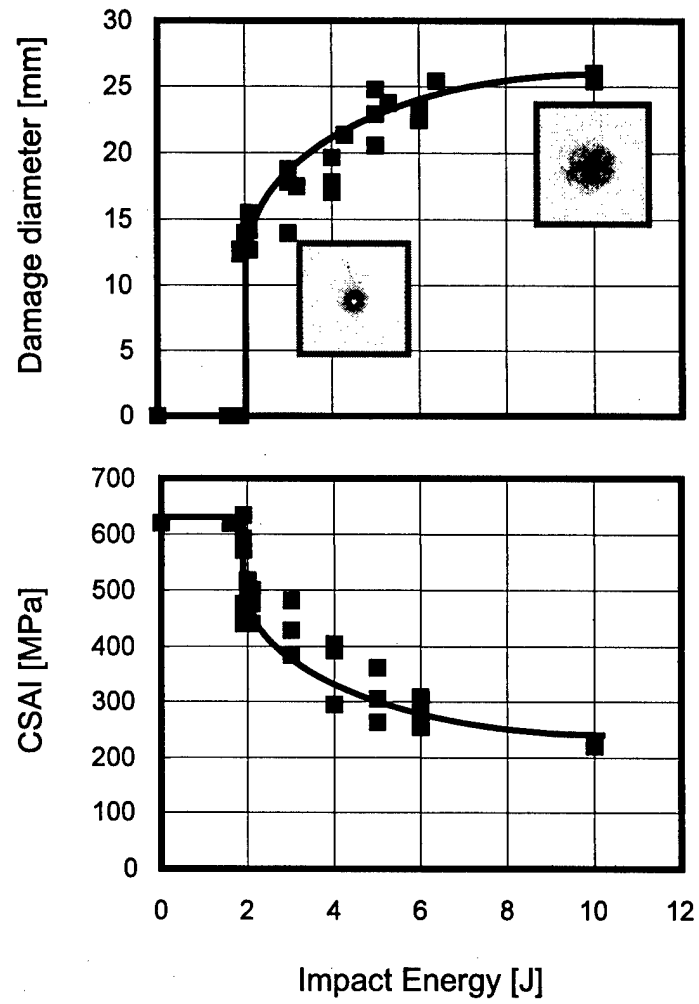FIGURE 4. FINITE ELEMENT MODELING PROCEDURE
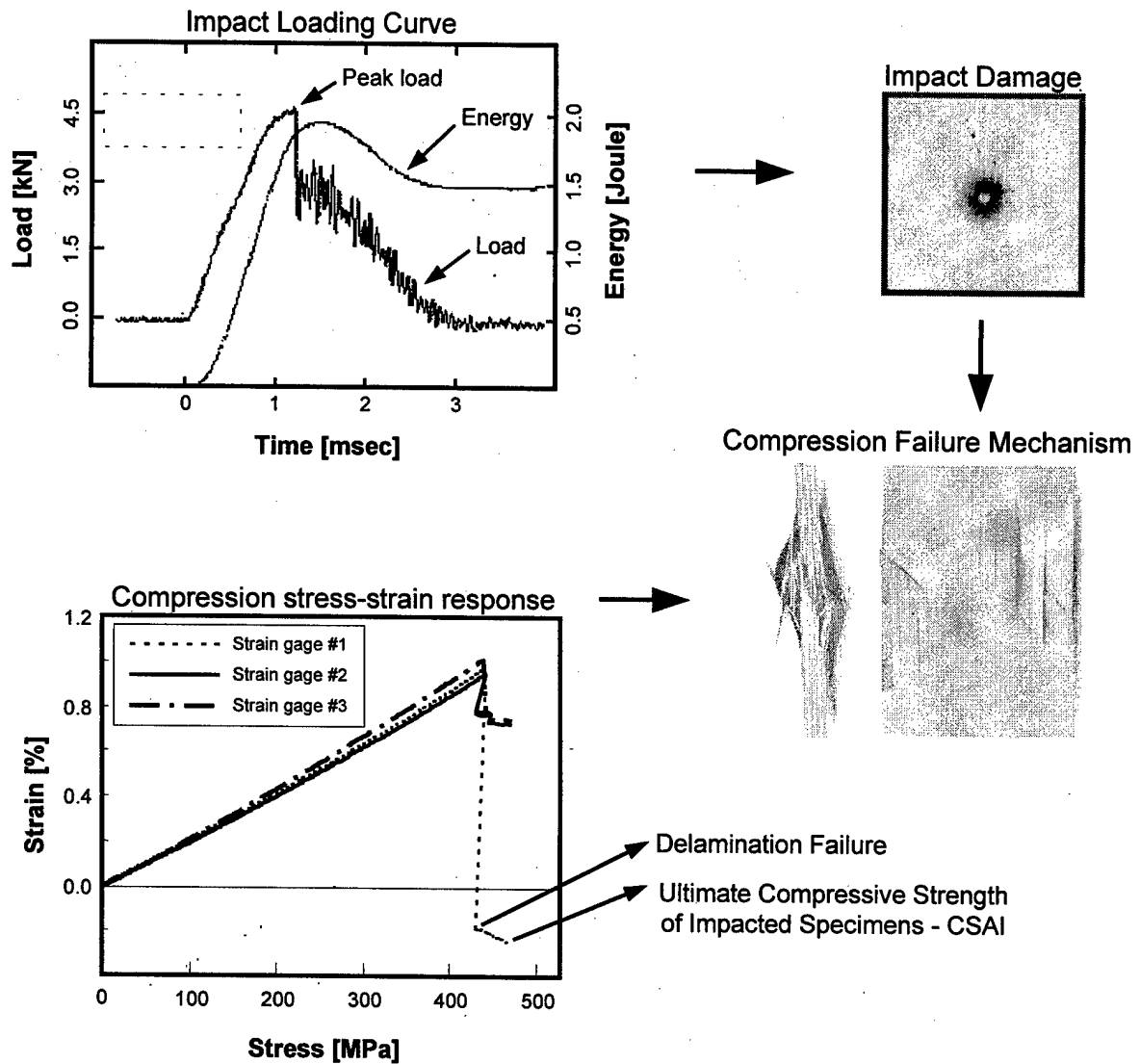
FIGURE 5. DAMAGE DIAMETER AND CSAI VS. THE INCIDENT
IMPACT ENERGY

FIGURE 6. IMPACT LOADING CURVES, INDUCED DAMAGE, AND FAILURE MECHANISMS FOR SAMPLE IMPACTED AT $E_i = 2J$ (12.7-mm DAMAGE DIAMETER)

Specimen 27E4
Ei = 1.5 J
50% of UTS

Specimen 27E5
Ei = 1.5 J
60% of UTS

Specimen 27E3
Ei = 1.9 J
50% of UTS

Specimen 27E7
Ei = 1.9 J
60% of UTS

N = 1,000,000

N = 500,000

N = 1,000,000

N = 500,000
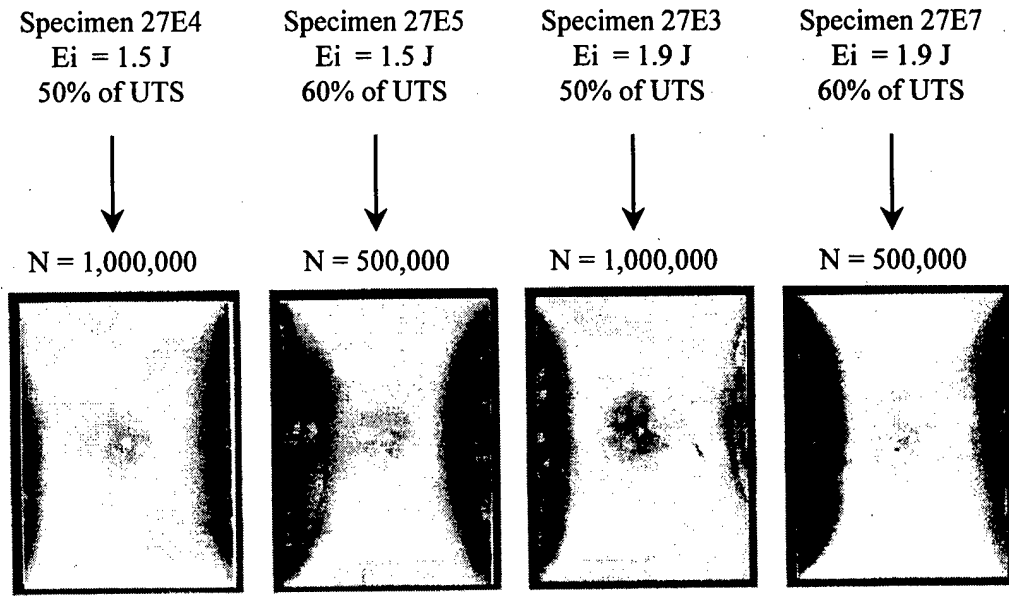
FIGURE 7. DAMAGE GROWTH UNDER TENSION-TENSION FATIGUE

Specimen 31C4

N = 0   N = 50,000   N = 100,000   N = 110,000

Specimen 33A5

N = 0   N = 50,000   N = 70,000   N = 70,500
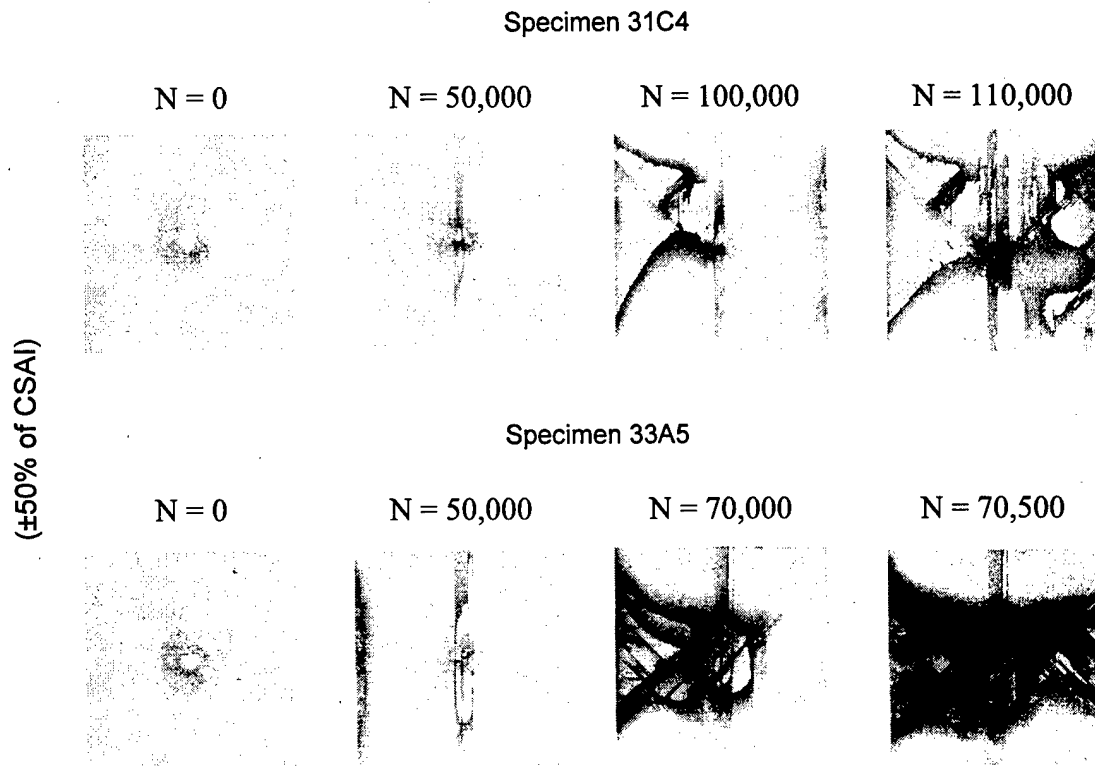
(±50% of CSAI)

FIGURE 8. DAMAGE GROWTH AS OBSERVED BY X-RAY RADIOGRAPHY
FOR CONSTANT-AMPLITUDE T-C LOADING (±50% OF CSAI)

Photograph of the Specimen During
Fatigue Loading

Specimen

Hydraulic Grips

N = 0   N = 1,000,000

Specimen 31D3

N = 0   N = 5,000   N = 500,000

Specimen 34A8
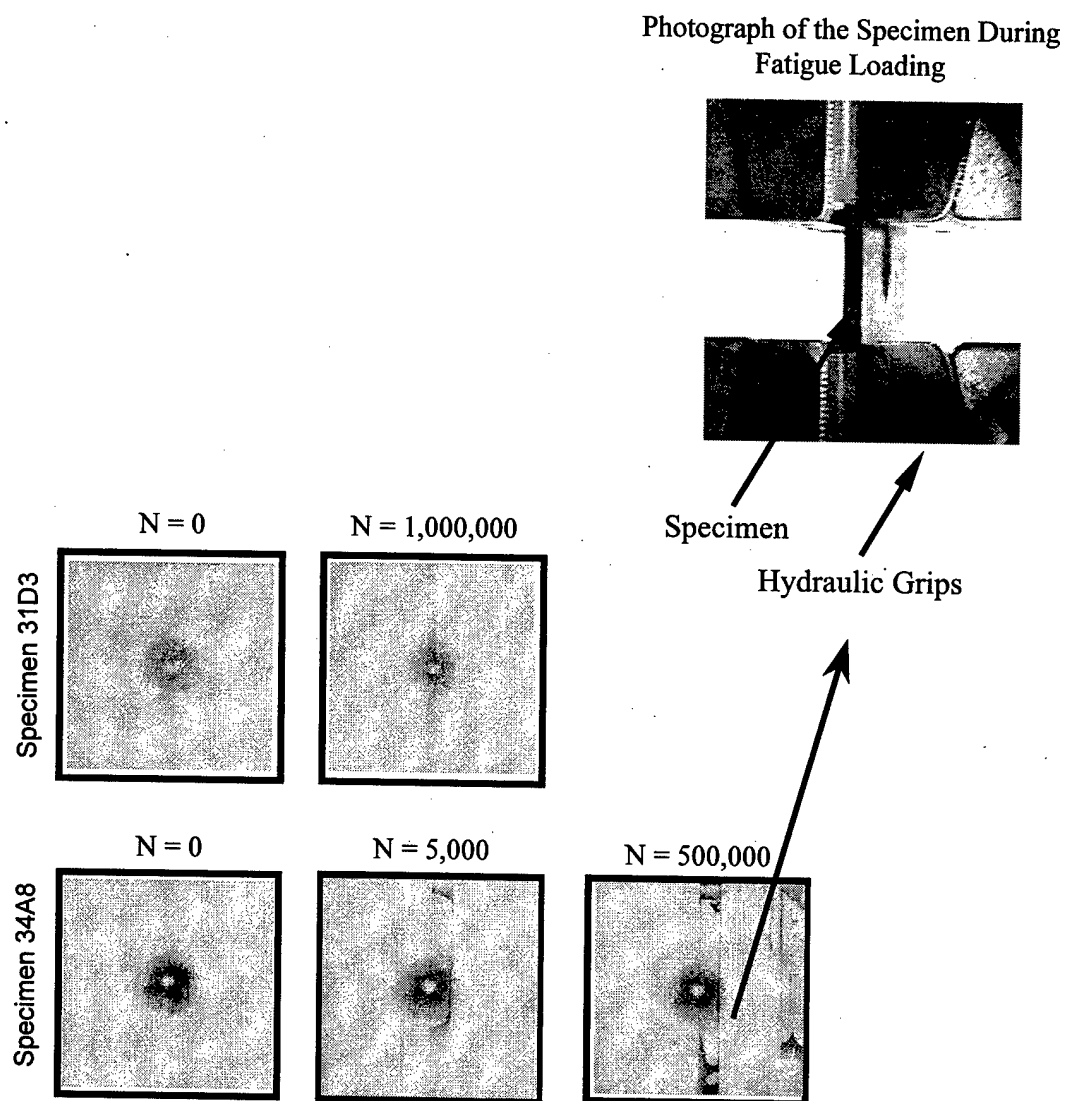
FIGURE 9. GROWTH OF IMPACT DAMAGE UNDER C-C FATIGUE (60% OF CSAI)
AND PHOTOGRAPH OF ONE SAMPLE DURING FATIGUE LOADING
INDICATING DELAMINATION GROWTH DUE TO THE BUCKLING OF
THIN DELAMINATED REGION

31

N = 10   N = 100   N = 1,000   N = 10,000

(70% of CSAI)

N = 10   N = 50   N = 100   N = 500

(80% of CSAI)

Failed After 587 Cycles

FIGURE 10. DAMAGE GROWTH AS OBSERVED BY X-RAY RADIOGRAPHY
FOR CONSTANT-AMPLITUDE C-C LOADING: 70% AND 80% CSAI

(a)

(b)

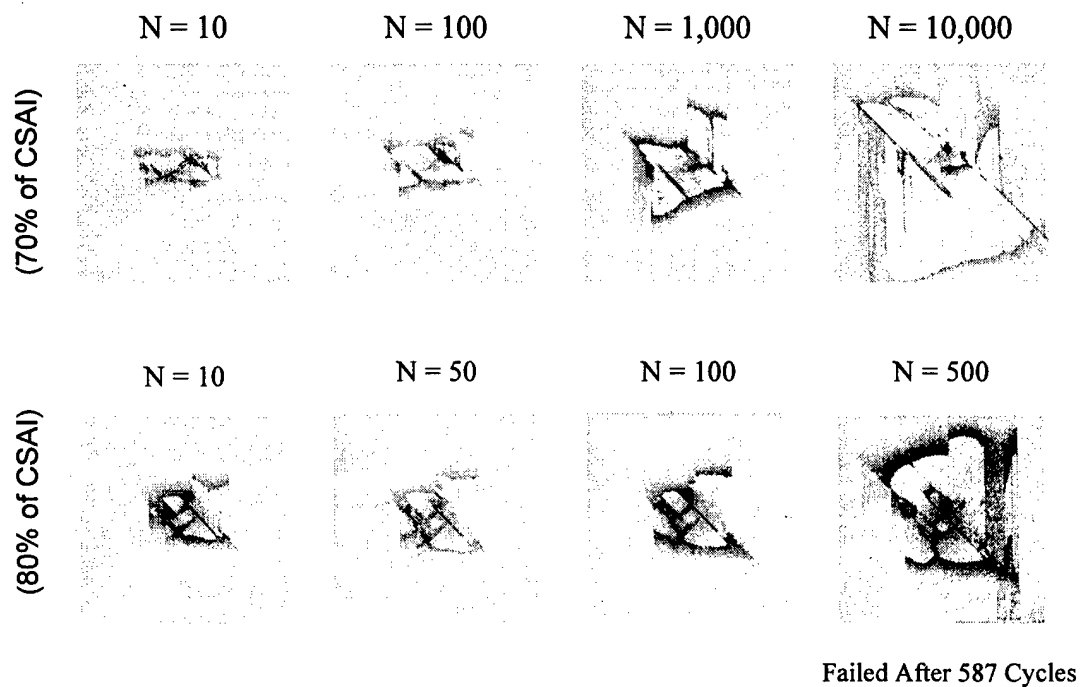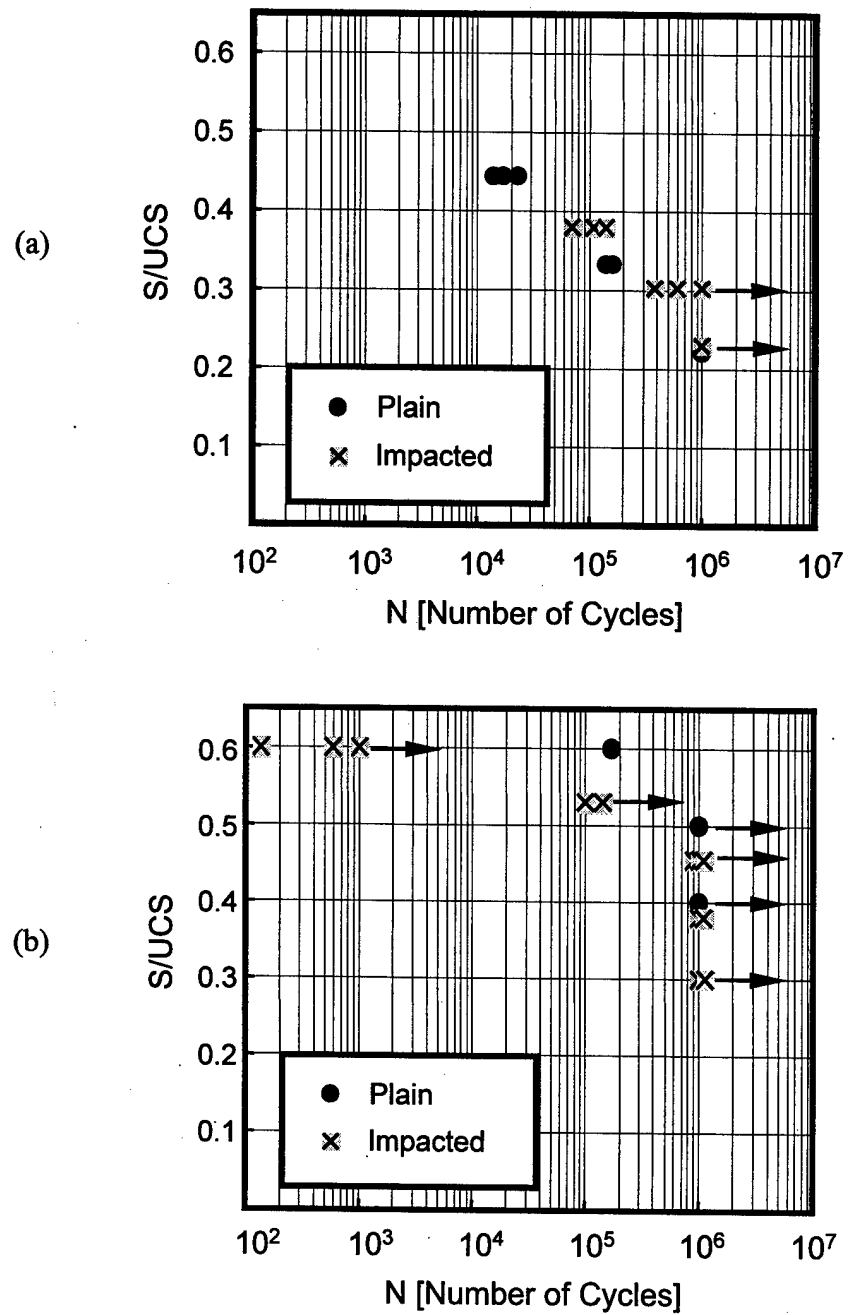FIGURE 11. NORMALIZED *S-N* CURVE FOR UNDAMAGED AND IMPACTED
SPECIMENS SUBJECTED TO (a) T-C AND (b) C-C LOADING (Note: Stress levels are
normalized with respect to the ultimate compressive strength (UCS) of undamaged specimens.)

33
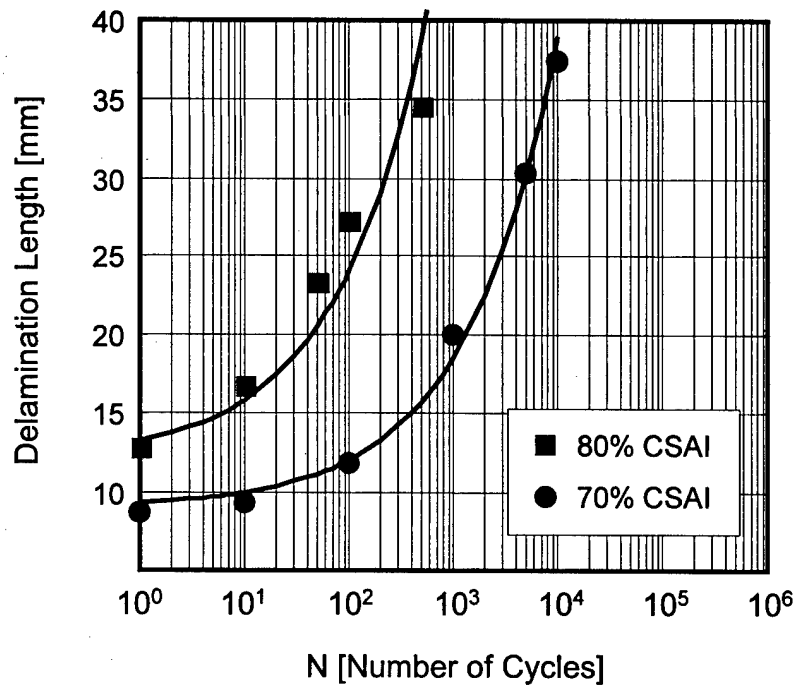
FIGURE 12. DAMAGE GROWTH IN CONSTANT-AMPLITUDE C-C FATIGUE AT 70% AND 80% CSAI AS A FUNCTION OF NUMBER OF CYCLES (AVERAGE OF THREE SPECIMENS)

N = 0

N = 1,000,000

10^6 cycles @ 40%

70%

N = 100   N = 1,000   N = 5,000   N = 10,000

FIGURE 13. GROWTH OF IMPACT DAMAGE UNDER TWO-LEVEL BLOCK
COMPRESSION-COMPRESSION LOADING (LOW/HIGH - 40/70% OF CSAI)
AS OBSERVED BY X-RAY RADIOGRAPHY

N = 0

100 cycles @ 70%

N = 100

40% R = infinity

N = 10,000   N = 100,000   N = 200,000   N = 500,000

FIGURE 14. GROWTH OF IMPACT DAMAGE UNDER TWO-LEVEL BLOCK
COMPRESSION-COMPRESSION LOADING (HIGH/LOW - 70/40% OF CSAI) AS
OBSERVED BY X-RAY RADIOGRAPHY

36

N = 0

N = 100

100 cycles @ 70%

60% R = infinity

N = 100

N = 1,000

N = 5,000

N = 10,000

FIGURE 15. GROWTH OF IMPACT DAMAGE UNDER TWO-LEVEL BLOCK
COMPRESSION-COMPRESSION LOADING (HIGH/LOW - 70/60% OF CSAI) AS
OBSERVED BY X-RAY RADIOGRAPHY

N = 0   N = 100

100 cycles @ 70%

30% R = infinity

N = 10,000   N = 100,000   N = 500,000   N = 1,000,000
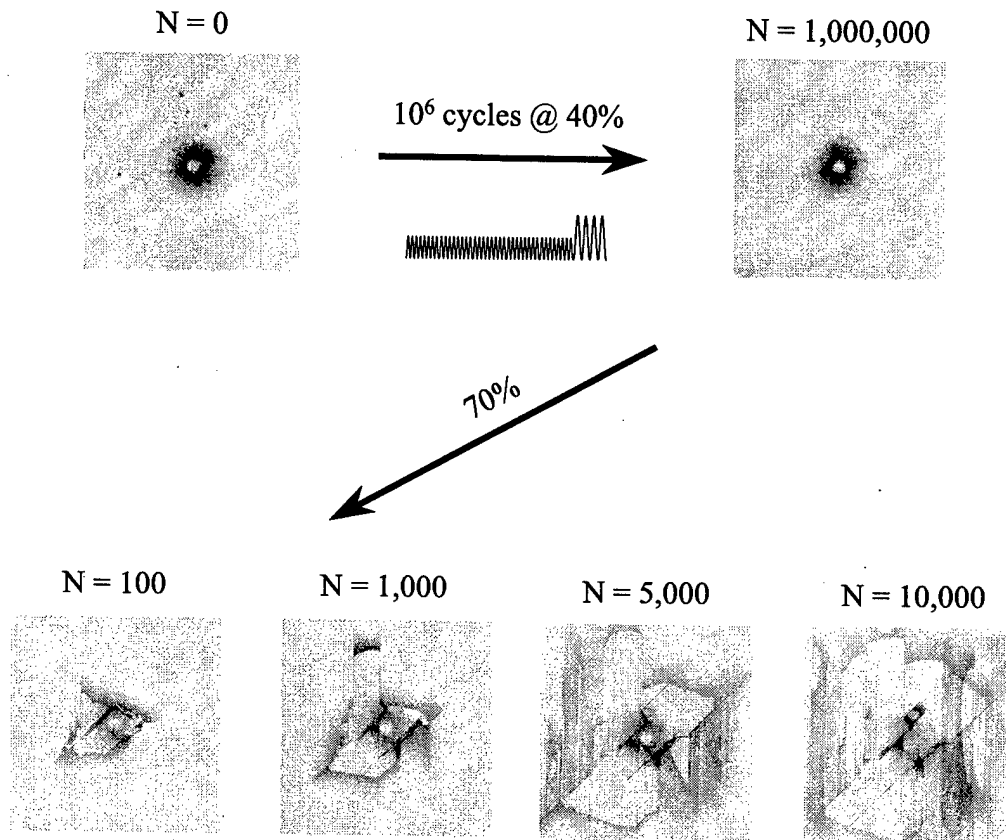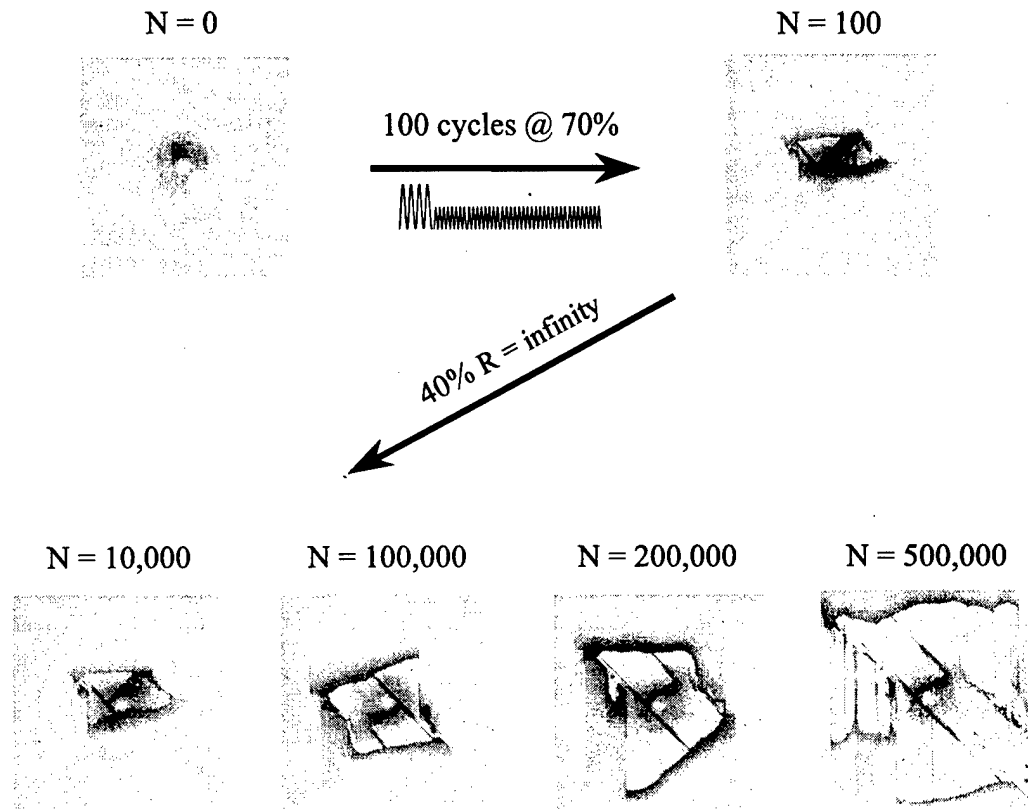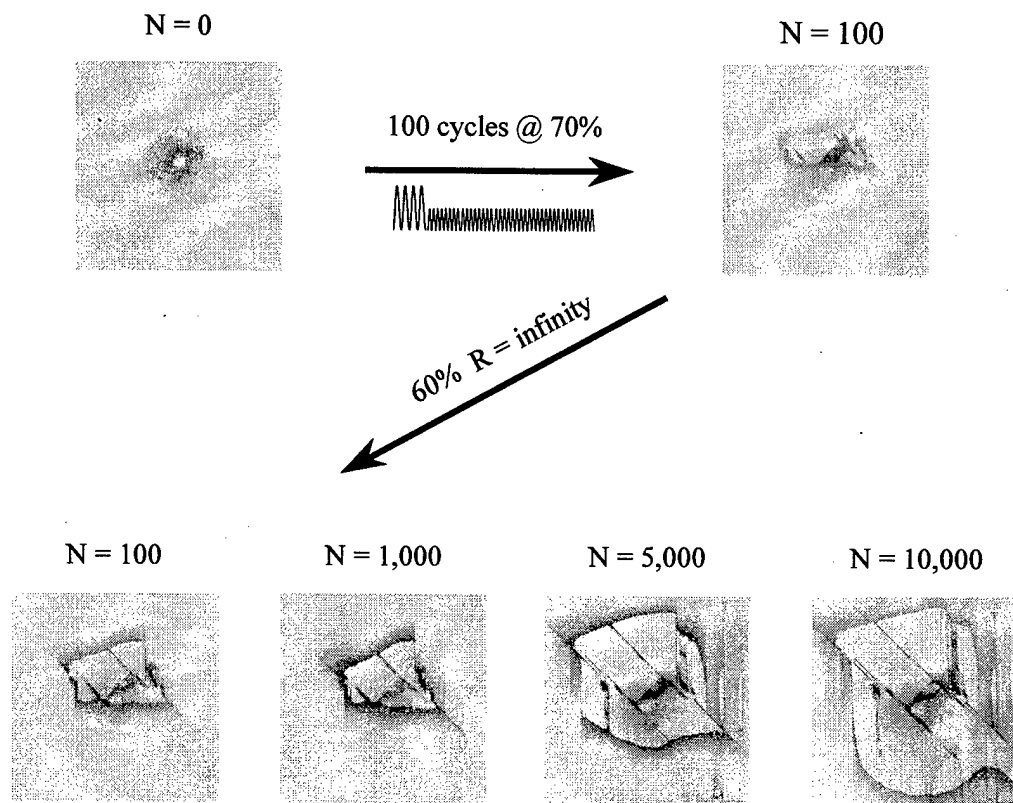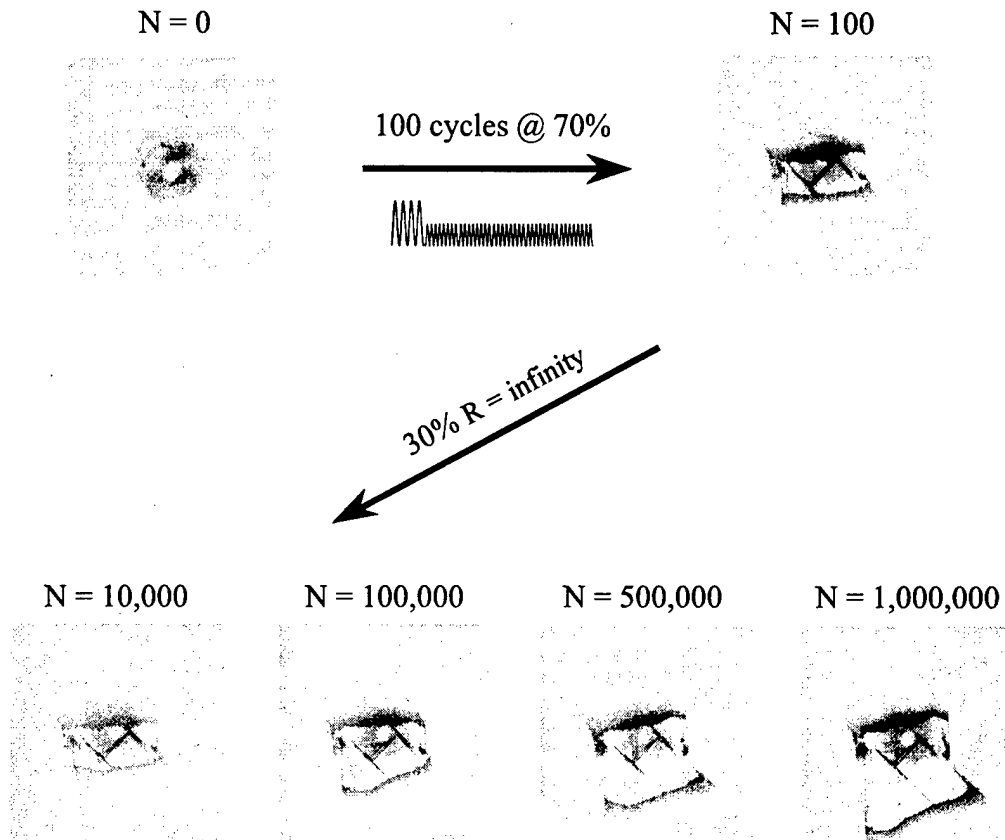
FIGURE 16. GROWTH OF IMPACT DAMAGE UNDER TWO-LEVEL BLOCK
COMPRESSION-COMPRESSION LOADING (HIGH/LOW - 70/30% OF CSAI) AS
OBSERVED BY X-RAY RADIOGRAPHY
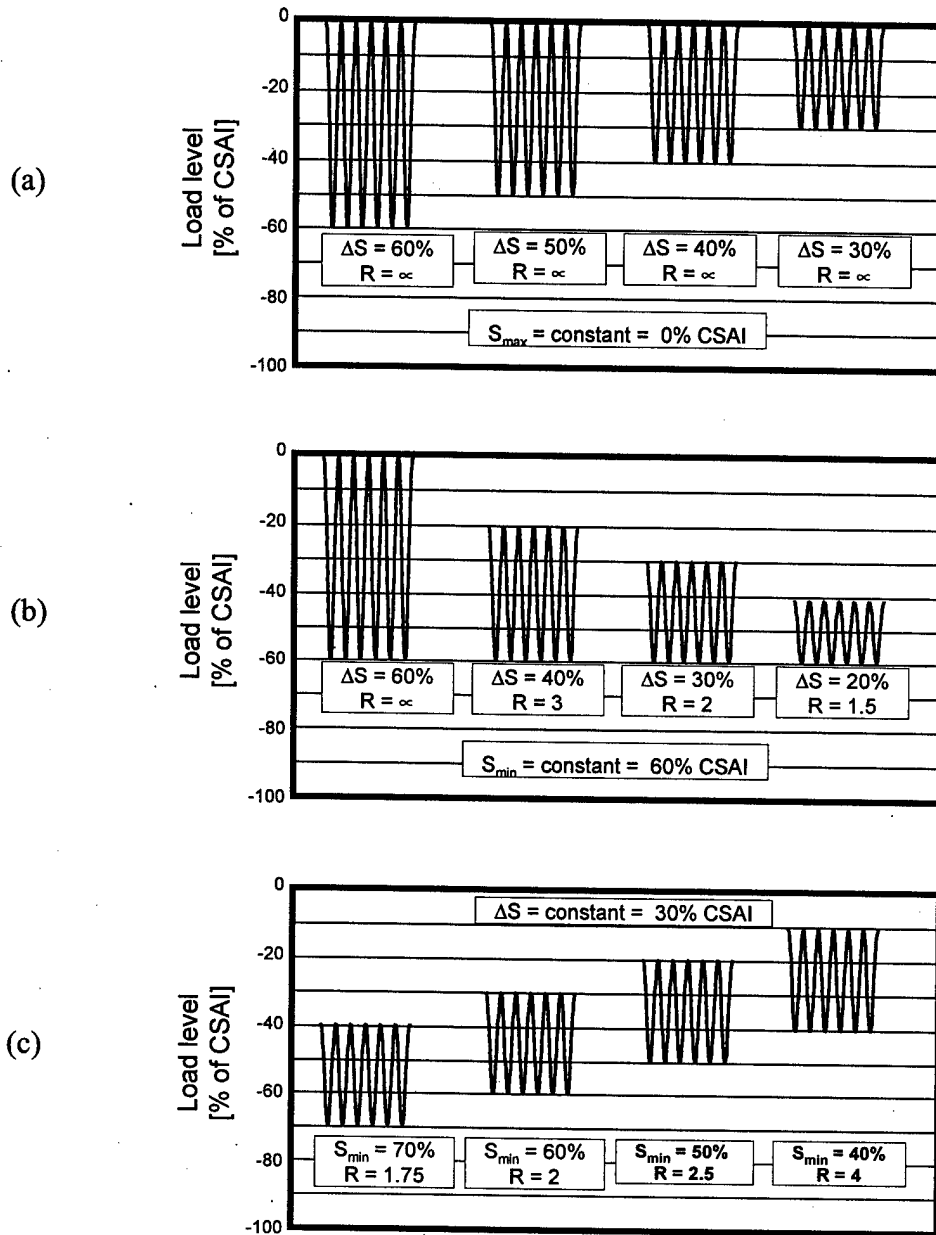
FIGURE 17. LOADING PARAMETERS (2nd BLOCK) IN HIGH/LOW BLOCK LOADING
(a) CONSTANT MAXIMUM LOAD, VARIABLE LOAD RANGE
S_{max} = constant = 0% CSAI ΔS = 30, 40, 50, 60 percent CSAI
(b) CONSTANT MINIMUM LOAD, VARIABLE LOAD RANGE
S_{min} = constant = 60% CSAI ΔS = 20, 30, 40, 60 percent CSAI
(c) CONSTANT LOAD RANGE, VARIABLE MINIMUM LOAD
ΔS = constant = 30% CSAI S_{min} = 40, 50, 60, 70 percent CSAI

(a)

(b)

(c)
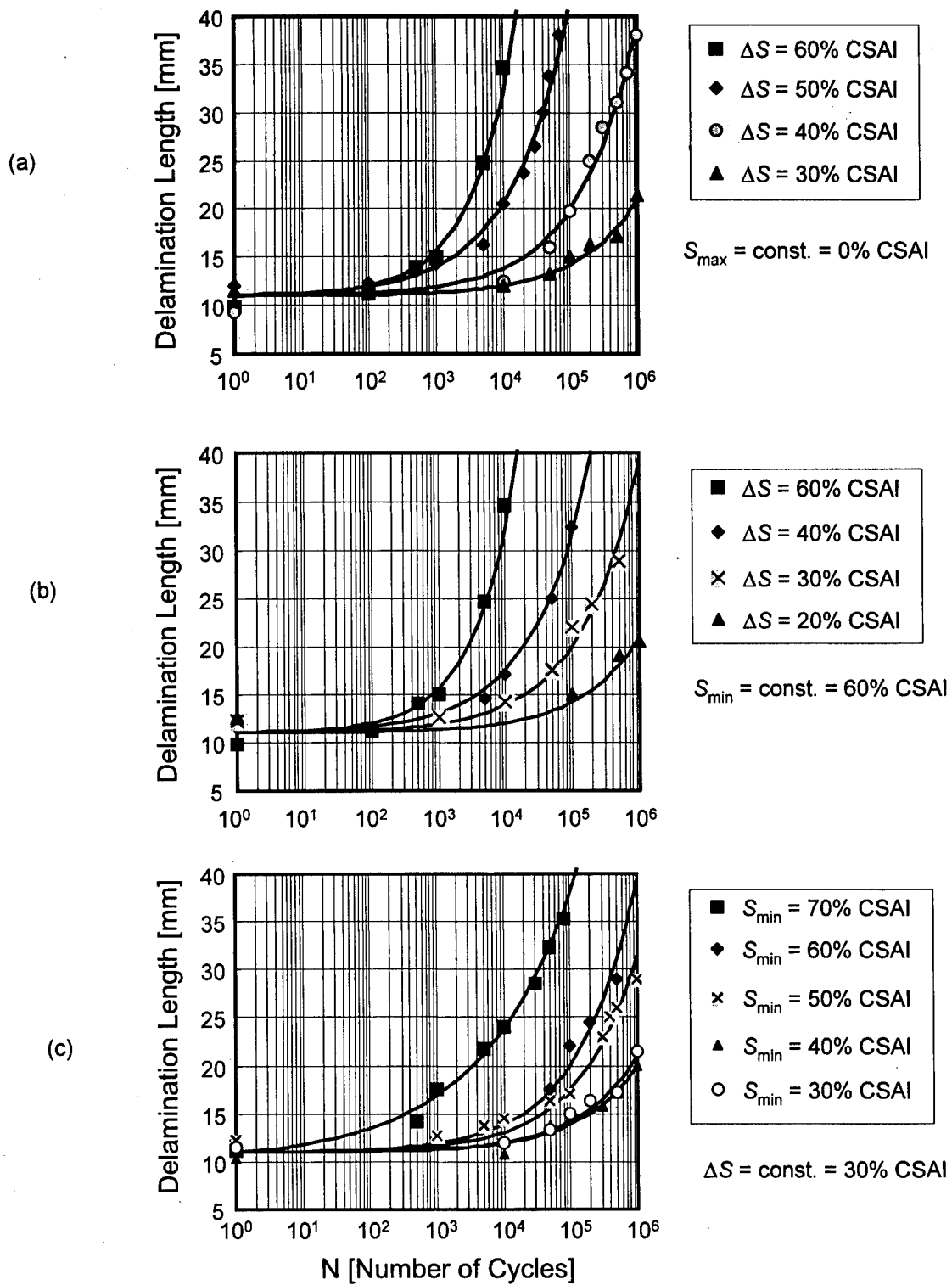
FIGURE 18. DELAMINATION LENGTH AS A FUNCTION OF N OF THE 2nd
BLOCK IN HIGH/LOW BLOCK LOADING (AVERAGE OF TWO SPECIMENS):
(a) CONSTANT MAXIMUM LOAD, VARIABLE LOAD RANGE
(b) CONSTANT MINIMUM LOAD, VARIABLE LOAD RANGE
(c) CONSTANT LOAD RANGE, VARIABLE MINIMUM LOAD

40
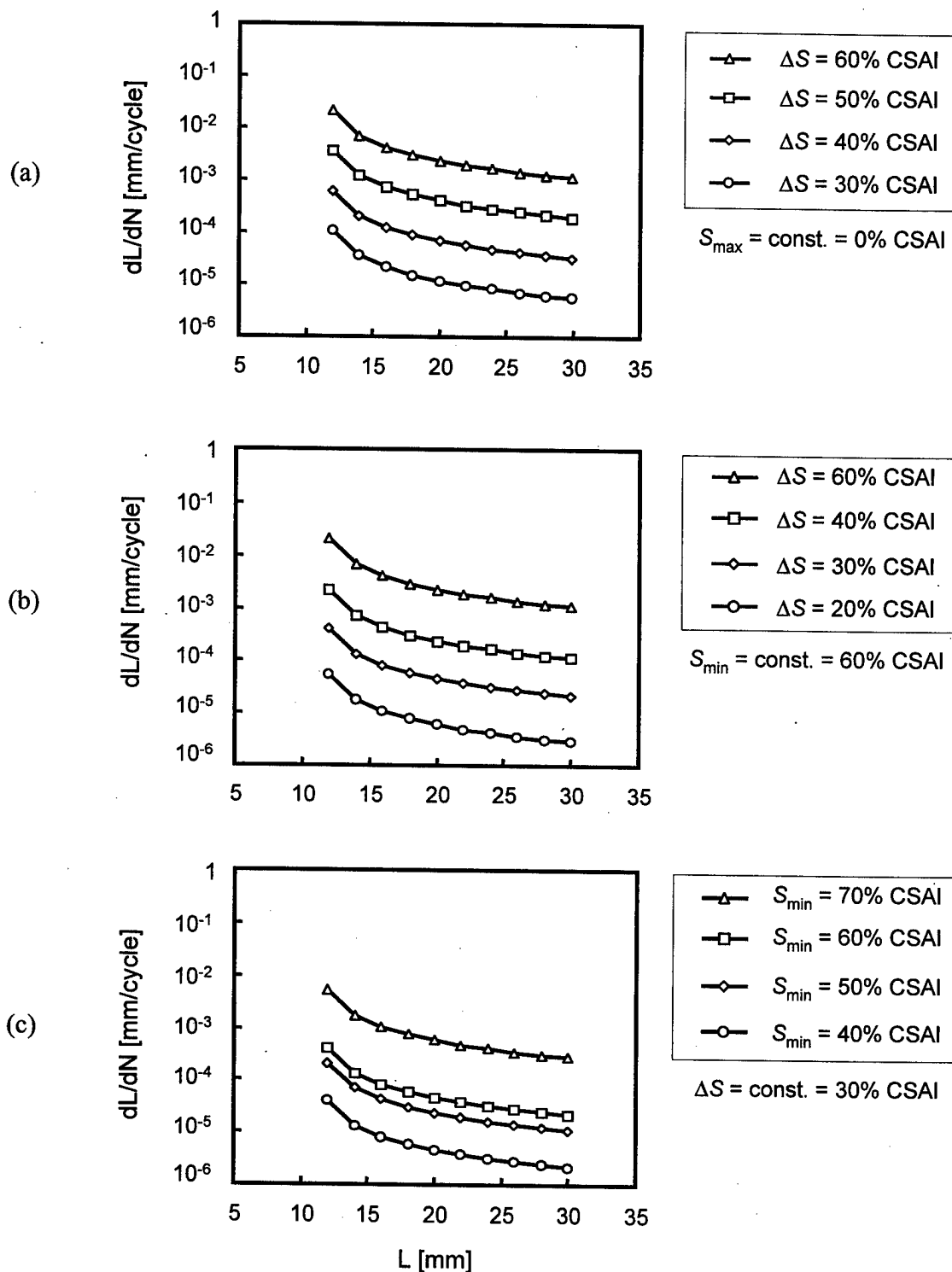
FIGURE 19. *dL/dN* AS A FUNCTION OF DELAMINATION LENGTH (*L*) FOR
HIGH/LOW BLOCK LOADING:
(a) CONSTANT MAXIMUM LOAD, VARIABLE LOAD RANGE
(b) CONSTANT MINIMUM LOAD, VARIABLE LOAD RANGE
(c) CONSTANT LOAD RANGE, VARIABLE MINIMUM LOAD

41
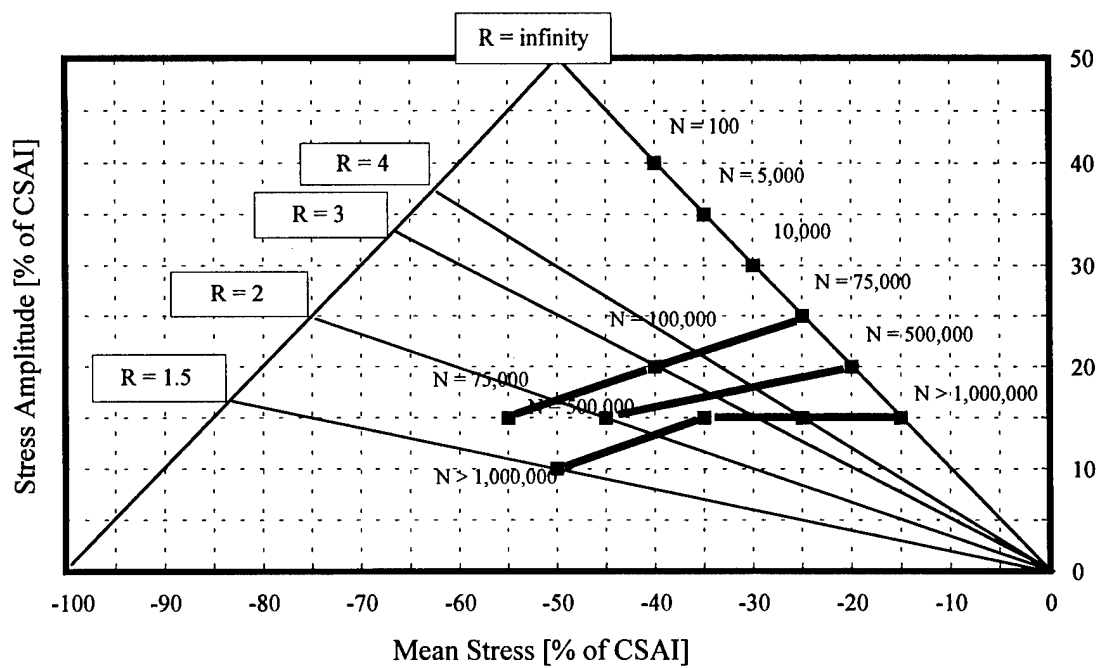
FIGURE 20. CONSTANT LIFE DIAGRAM

Initial impact damage

After 2 load levels from block 1 (3 cycles)

After 4 load levels from block 1 (26 cycles)

After 6 load levels from block 1 (230 cycles)

After 8 load levels from block 1 (5200 cycles)

After 10 load levels from block 1 (398,665 cycles)

After 2 blocks (~800,000 cycles)

After 4 blocks (~1,600,000 cycles)

After 6 blocks (~2,400,000 cycles)

After 8 blocks (~3,200,000 cycles)

After 10 blocks (~4,000,000 cycles)

FIGURE 21. DAMAGE GROWTH AS A FUNCTION OF COMPLETED LOAD LEVELS WITHIN 1 BLOCK AND AS A FUNCTION OF COMPLETED BLOCKS (FULL TWIST SPECTRUM, FML = 27.5% CSAI)

43

Full TWIST

(a)

| Specimen 33F5 | Specimen 33E6 | Specimen 33F2 |

Modified TWIST

(b)

| Specimen 31D6 | Specimen 33E7 | Specimen 33C5 |
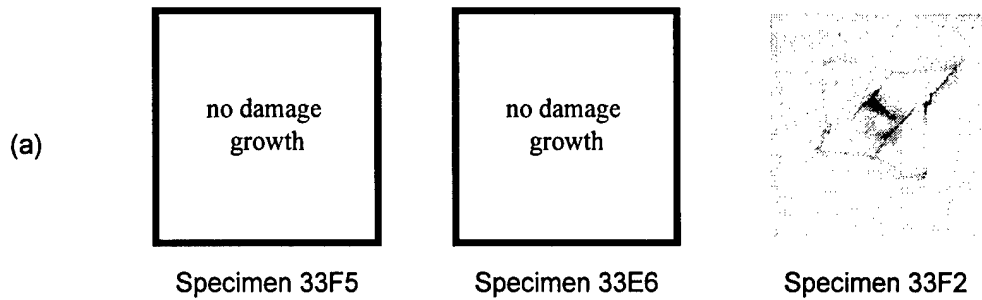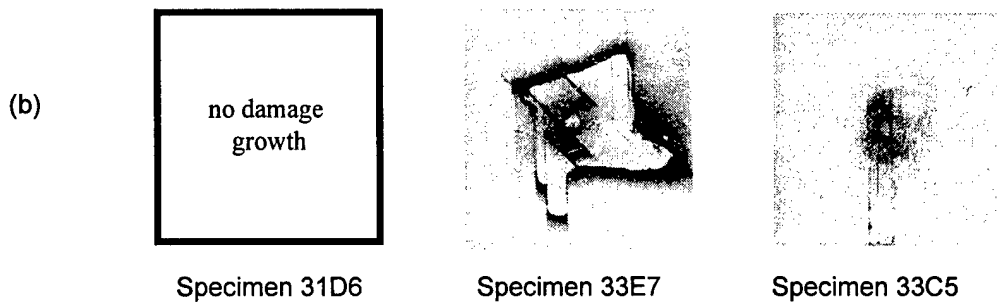
FIGURE 22. FINAL DAMAGE PATTERNS AFTER 10 BLOCKS OF TWIST LOADING AT
27.5% OF CSAI FLIGHT MEAN (a) FULL AND (b) MODIFIED SPECTRUM

Full TWIST
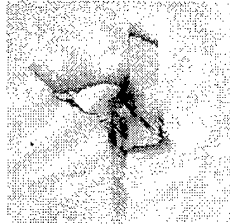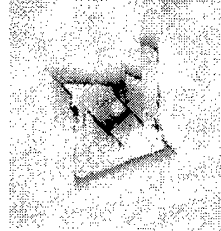
Specimen 31A5   Specimen 31A6   Specimen 33F1
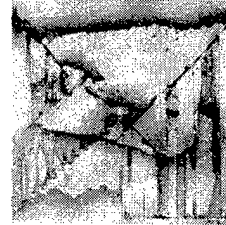
Modified TWIST
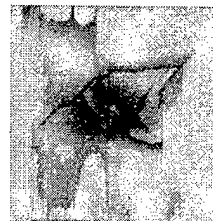
Specimen 31D2   Specimen 33C4   Specimen 33C2
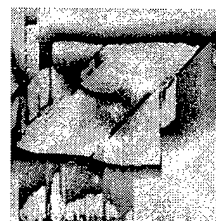
FIGURE 23. FINAL DAMAGE PATTERNS AFTER 10 BLOCKS OF TWIST LOADING AT
30% OF CSAI FLIGHT MEAN (a) FULL AND (b) MODIFIED SPECTRUM
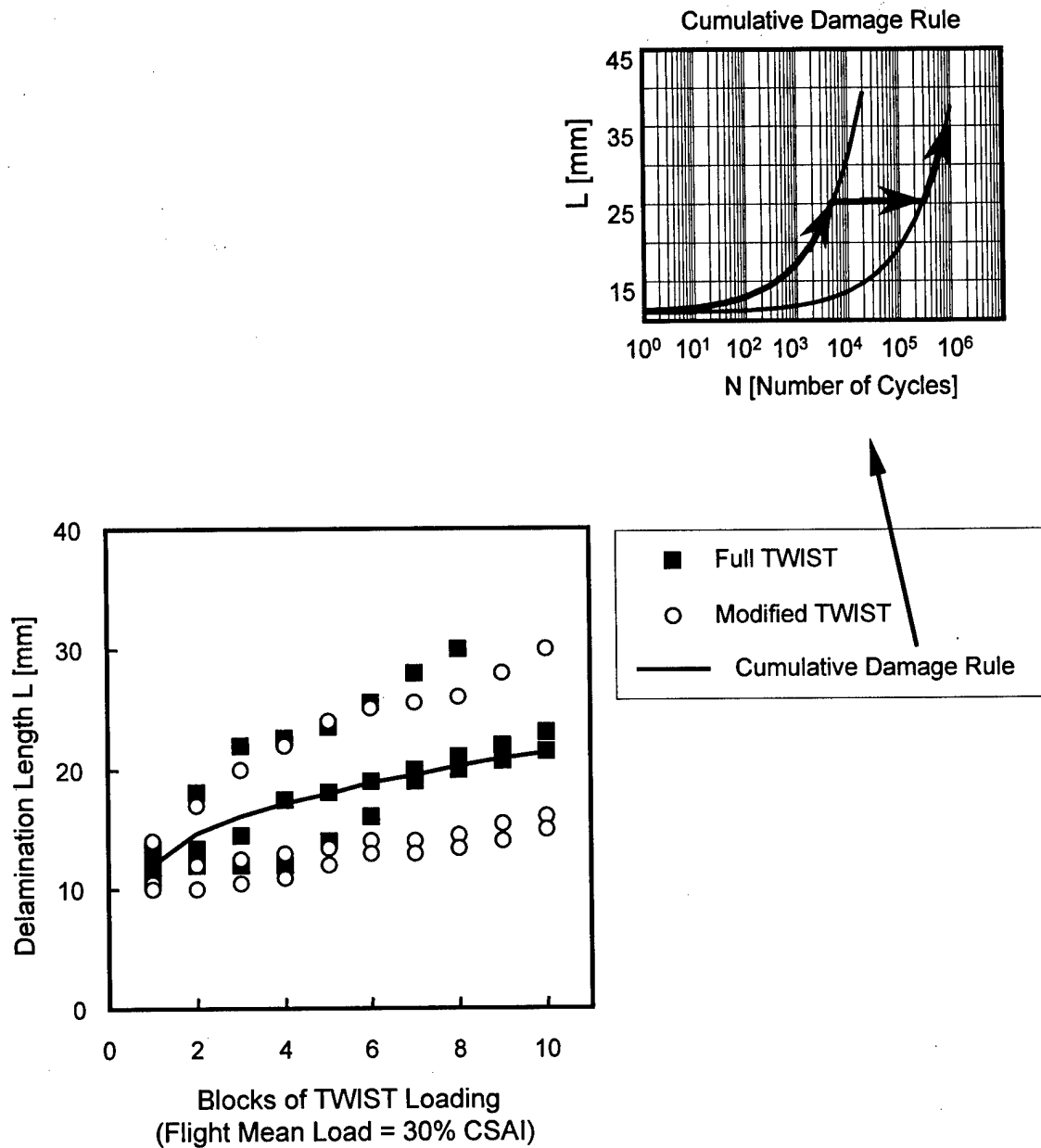
FIGURE 24. DELAMINATION GROWTH AS A FUNCTION OF COMPLETED BLOCKS
FOR (a) FULL AND (b) MODIFIED SPECTRUM AT FLIGHT MEAN OF 30% OF CSAI
(Comparison between cumulative damage model prediction and experimental data.)

CSAI = 470 MPa
(± 30 MPa)

Specimen 31A6   Specimen 33B5

Damage Patterns After Fatigue
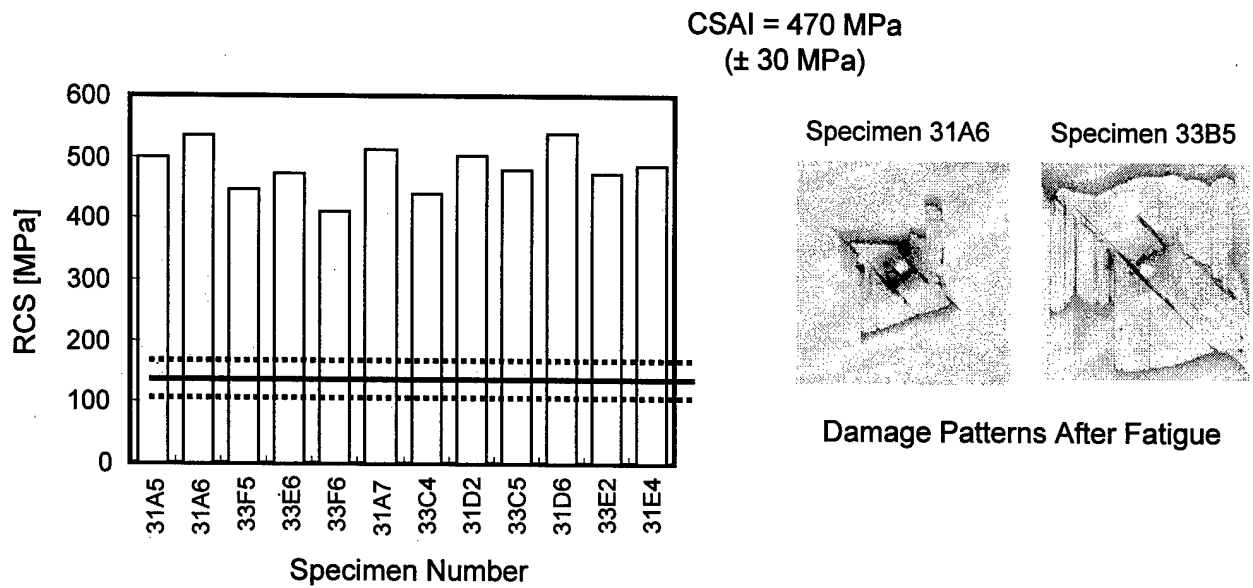
(a) Specimens Tested in Spectrum Fatigue

CSAI = 470 MPa
(± 30 MPa)
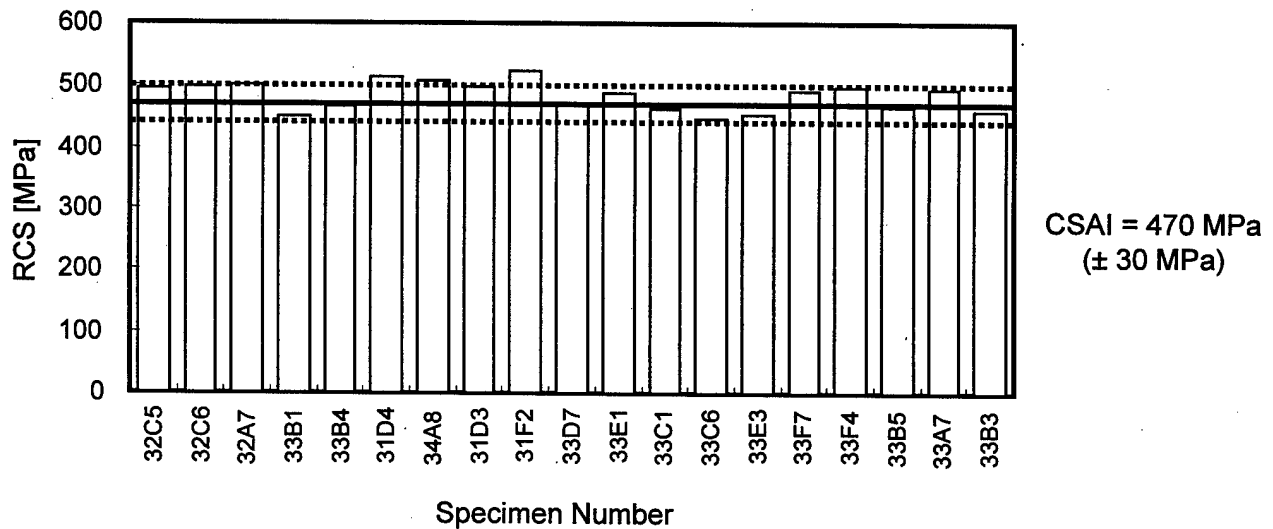
(b) Specimens Tested in Constant-Amplitude C-C and Two-Level Block Loading

FIGURE 25. RESIDUAL COMPRESSIVE STRENGTH (RCS)
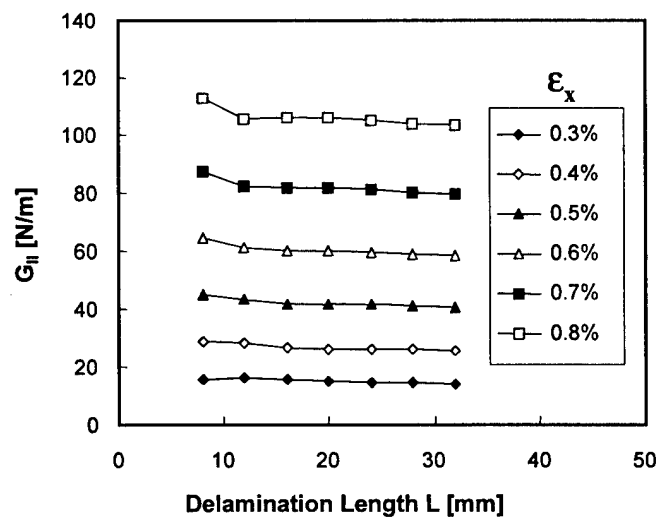
FIGURE 26. STRAIN ENERGY RELEASE RATES (G_{II}) AS A FUNCTION OF
APPLIED LOAD (ε_X IN %) AND DELAMINATION LENGTH (L) FOR
DELAMINATION LOCATED BETWEEN PLIES 1 AND 2
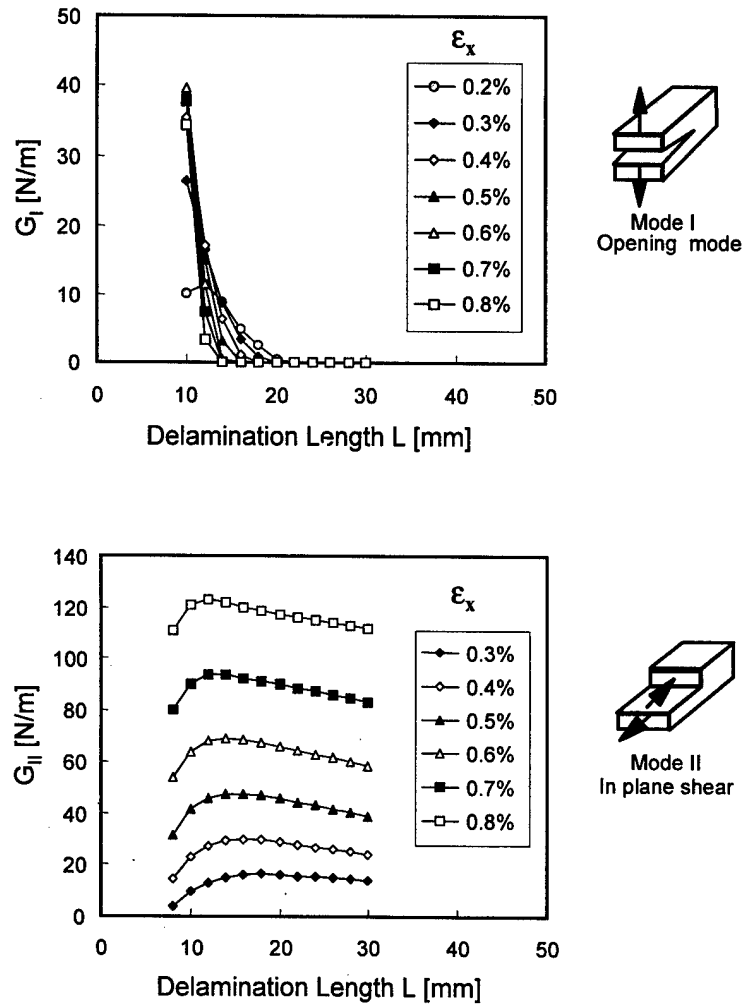
FIGURE 27. STRAIN ENERGY RELEASE RATES (G_I AND G_{II}) AS A
FUNCTION OF APPLIED LOAD (ε_x IN %) AND DELAMINATION LENGTH (L)
FOR DELAMINATION LOCATED BETWEEN PLIES 2 AND 3

49
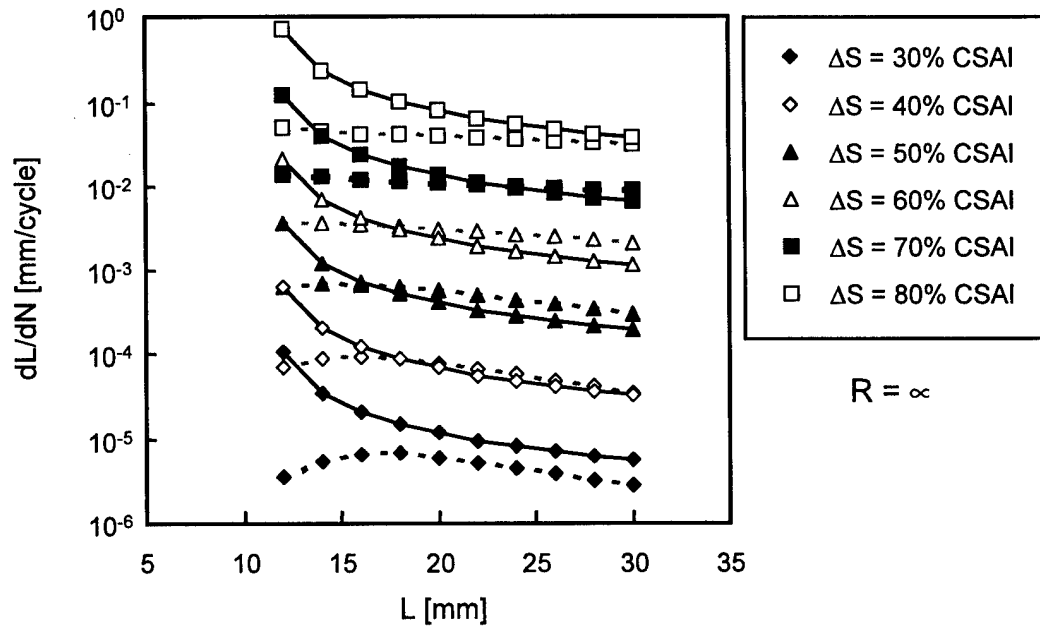
FIGURE 28. CYCLIC GROWTH RATES (*dL/dN*) IN CONSTANT-AMPLITUDE
C-C LOADING AS A FUNCTION OF *L* (solid lines - experimental data, dashed lines -
analytical prediction): S_{max} = constant = 0% CSAI, ΔS = 30, 40, 50, 60, 70, 80 percent CSAI
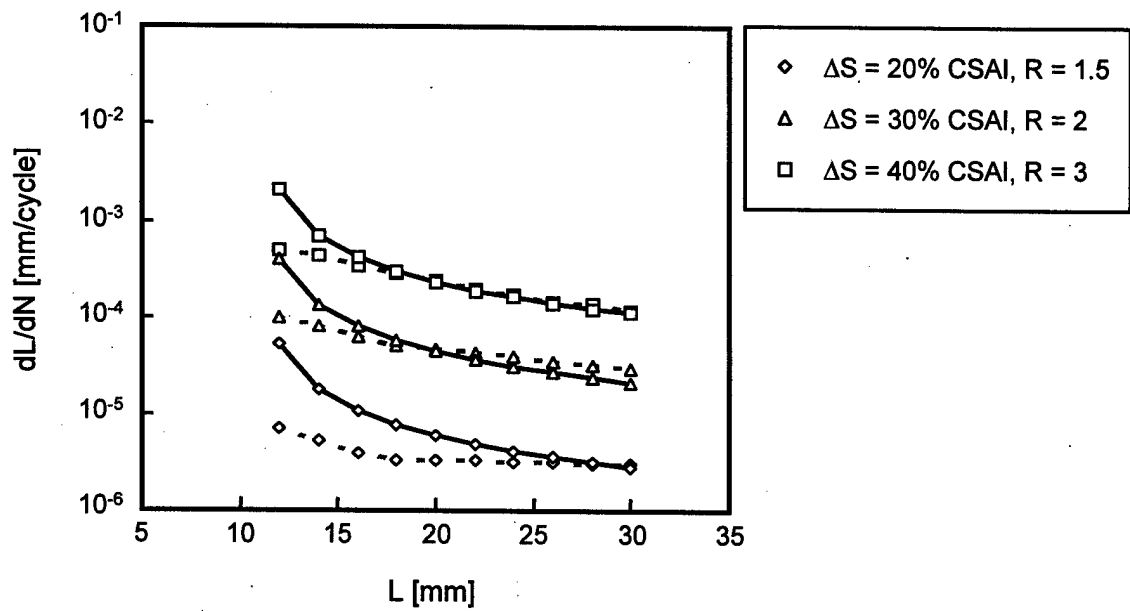
FIGURE 29. CYCLIC GROWTH RATES (dL/dN) IN CONSTANT-AMPLITUDE C-C
LOADING AS A FUNCTION OF L (solid lines - experimental data, dashed lines -
analytical prediction): S_{min} = constant = 60% CSAI, ΔS = 20, 30, 40 percent CSAI
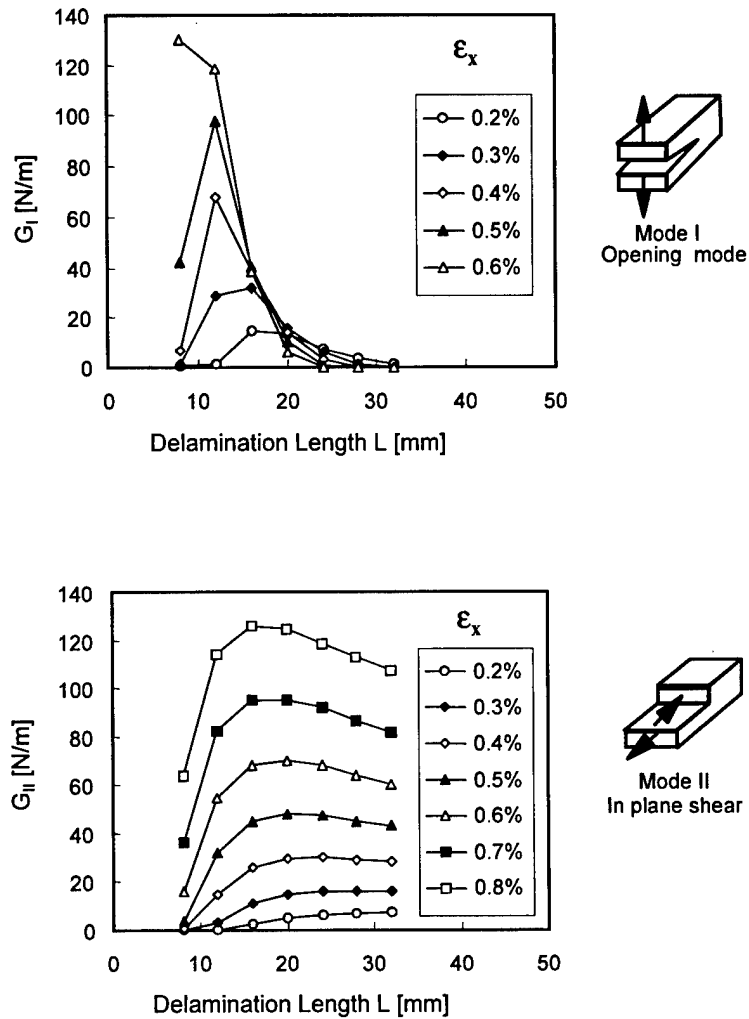
FIGURE 30. STRAIN ENERGY RELEASE RATES (G_I AND G_{II}) AS A FUNCTION OF APPLIED LOAD (ε_x IN %) AND DELAMINATION LENGTH (L) FOR DELAMINATION LOCATED BETWEEN PLIES 3 AND 4

52

TABLE 1. TRANSPORT WING STANDARD TEST SPECTRUM (TWIST)

Flight Type	Frequency of Each Flight Type in One Block of 4000 Flights	Frequency of Occurrence of Flight Load Cycles at 10 Alternating Load Levels										Total Number of Cycles per Flight	Total Number of Cycles at Flight	Percent of Total Cycles
		1.6	1.5	1.3	1.1	0.99	0.84	0.68	0.53	0.37	0.22			
A	1	1	1	1	4	8	18	64	112	391	900	1500	1500	0.38%
B	1		1	1	2	5	11	39	76	366	899	1400	1400	0.35%
C	3			1	1	2	7	22	61	277	879	1250	3750	0.94%
D	9				1	1	2	14	44	208	680	950	8550	2.14%
E	24					1	1	6	24	165	603	800	19200	4.82%
F	60						1	3	19	115	512	650	39000	9.78%
G	181							1	7	70	412	490	88690	22.2%
H	420								1	16	233	250	105000	26.3%
I	1090									1	69	70	76300	19.1%
J	2211										25	25	55275	13.8%
Total Number of Load Cycles/Block of 4000 Flights		1	2	5	18	52	152	800	4170	34800	358665		398665	100%

TABLE 2. UNIDIRECTIONAL LAMINA (PLY) PROPERTIES FOR AS4/3501-6

E_{11} (GPa)	139.1
E_{22} (GPa)	9.20
G_{12} (GPa)	5.28
ν_{12}	0.28
ply thickness (mm)	0.125

TABLE 3. SUMMARY OF IMPACT AND STATIC COMPRESSION TEST RESULTS

Specimen Number	Initial Impact E [J]	Damage Diameter [mm]	CSAI [MPa]
No impact (average of 5 specimens)	0	0	621
33a7	1.9	0	593
32c3	1.9	0	572
31c5	1.9	0	634
31c2	1.9	12.4	477
31c3	1.9	12.7	440
33a4	1.9	12.7	471
31d3	2.0	14.0	495
31e3	2.0	12.7	455
33e3	2.0	13.7	519
35a6	2.1	13.2	468
35a5	2.1	13.7	471
32c7	2.1	15.5	501
34a8	2.1	15.0	484
33a2	2.1	13.2	486
31c1	2.1	12.7	440
31d7	3.0	18.8	430
31e7	3.0	17.8	385
33e7	3.0	14.0	483
31d6	4.0	19.7	405
31e6	4.0	17.1	297
33e6	4.0	17.8	393
31d5	5.0	20.6	306
31e5	5.0	22.9	264
33e5	5.0	24.8	362
31d4	6.0	22.5	286
31e4	6.0	23.2	255
33e4	6.0	23.4	310
31d2	10.0	25.7	221
31e2	10.0	25.4	221
33e2	10.0	26.0	231

TABLE 4. TEST MATRIX FOR CONSTANT-AMPLITUDE LOADING

Constant-Amplitude Tension-Tension

Specimen Number	Load Level [% of UTS] R = 0.1	E$_i$ in Joules (Damage D in Inches)	N Number of Cycles	Impact-Induced Damage Growth
27E4	50%	1.5 J (0.5")	1,000,000	no
27E5	60%	1.5 J (0.5")	500,000	no
27E3	50%	1.9 J (0.6")	1,000,000	no
27E7	60%	1.9 J (0.6")	500,000	no

Constant-Amplitude Tension-Compression (R = -1)

Specimen Number	Load Level [% of CSAI]	N Number of Cycles	Impact-Induced Damage Growth	RCS [MPa]
32C5	±30%	1,000,000	no	496
32C6	±30%	1,000,000	no	498
33E5	±30%	1,000,000	no	-
31C5	±40%	>600,000	no	-
31F4	±40%	1,000,000	no	-
33A6	±40%	376,602*	no	-
31F7	±50%	140,000*	no	-
33A5	±50%	70,500*	no	-
31C4	±50%	110,000 *	no	-

Constant-Amplitude Compression-Compression (R = ∞)

Specimen Number	Load Level [% of CSAI]	N Number of Cycles	Impact-Induced Damage Growth	RCS [MPa]
32A6	40%	1,000,000	no	-
32A7	40%	1,000,000	no	500
31C7	40%	1,000,000	no	-
33B1	50%	1,000,000	no	450
31D4	50%	1,000,000	no	515
33B4	50%	1,000,000	no	467
31E5	60%	1,000,000	no	-
34A8	60%	>500,000	yes	507
31D3	60%	1,000,000	no	499
33B2	70%	141,607*	yes	-
31F2	70%	>10,000**	yes	522
35A6	70%	>100,000	yes	-
33F3	80%	136*	yes	-
31E1	80%	587*	yes	-
33C3	80%	>1,000	yes	-

* indicates cycles to final failure
** indicates number of cycles that causes propagation of delamination to the tab region

TABLE 5. TEST MATRIX FOR CONSTANT-AMPLITUDE C-C TWO-LEVEL BLOCK LOADING

Block Loading (Low/High) (R = ∞)

Specimen Number	Maximum Compressive Load S_{min} [% CSAI]	Load Range ΔS [% CSAI]	N [Number of Cycles]	RCS [MPa]
31C7	40% (low)	40%	1,000,000	-
	70% (high)	70%	>500,000	
32A6	40% (low)	40%	1,000,000	-
	70% (high)	70%	45,296*	

Block Loading (High/Low)

Loading Parameters for the Second Block (low)

First Block (high): 100 Cycles at 70% CSAI (R=∞)

Specimen Number	Maximum Compressive Load S_{min} [% CSAI]	Load Range ΔS [% CSAI]	N [Number of Cycles]	RCS [MPa]
(33D1 & 33D7)	70%	30%	75,000**	473
(33E1 & 31E7)	60%	60%	10,000**	488
(33C1 & 31E6)	60%	40%	100,000**	464
(33C6 & 31E3)	60%	30%	500,000**	446
(33E3 & 31E2)	60%	20%	1,000,000	452
(33C7 & 33F7)	50%	50%	75,000**	490
(33F4 & 31D7)	50%	30%	1,000,000	498
(33B5 & 31F6)	40%	40%	500,000**	465
(33A7 & 31D5)	40%	30%	1,000,000	496
(33B3 & 31D1)	30%	30%	1,000,000	461

* Indicates cycles to final failure.

** Indicates number of cycles that causes propagation of delamination to the tab region.

56

TABLE 6. BEST-FIT PARAMETERS (a, b, c) FOR DELAMINATION GROWTH CURVES (EQUATION 3)

	Best fit parameters		
Loading (% of CSAI)	a	b	c
S_{min} = 80% (ΔS = 80%)	12	1.200	0.5
S_{min} = 70% (ΔS = 70%)	9	0.300	0.5
S_{min} = 70% (ΔS = 30%)	10.2	0.790	0.31
S_{min} = 60% (ΔS = 60%)	11	0.048	0.66
S_{min} = 60% (ΔS = 40%)	11	0.065	0.5
S_{min} = 60% (ΔS = 30%)	11	0.028	0.5
S_{min} = 60% (ΔS = 20%)	11	0.010	0.5
S_{min} = 50% (ΔS = 50%)	11	0.095	0.5
S_{min} = 50% (ΔS = 30%)	11	0.020	0.5
S_{min} = 40% (ΔS = 40%)	11	0.028	0.5
S_{min} = 40% (ΔS = 30%)	11	0.009	0.5
S_{min} = 30% (ΔS = 30%)	11	0.010	0.5

TABLE 7. LOAD LEVELS IN PERCENT CSAI ASSOCIATED WITH THREE DIFFERENT FLIGHT MEAN LOAD (FML) LEVELS OF TWIST SPECTRUM

Load Level Number	S_{min}/S_{mean}	Cumulative Number of Cycles in 1 Block	TWIST Flight Mean Load - S_{mean} FML [% CSAI]								
			-30%			-27.5%			-25%		
			max	min	ΔS	max	min	ΔS	max	min	ΔS
			[% CSAI]								
1	2.6	1	18	-78	96	17	-72	88	15	-65	80
2	2.5	2	15	-75	90	14	-69	83	13	-63	75
3	2.3	5	9	-69	78	8	-63	72	8	-58	65
4	2.15	18	5	-65	69	4	-59	63	4	-54	58
5	1.99	52	0	-60	59	0	-55	54	0	-50	50
6	1.84	152	-5	-55	50	-4	-51	46	-4	-46	42
7	1.68	800	-10	-50	41	-9	-46	37	-8	-42	34
8	1.53	4170	-14	-46	32	-13	-42	29	-12	-38	27
9	1.37	34800	-19	-41	22	-17	-38	20	-16	-34	19
10	1.22	358665	-23	-37	13	-21	-34	12	-20	-31	11

TABLE 8. TEST MATRIX FOR COMPRESSION-DOMINATED BLOCKED TWIST LOADING

Full-Spectrum Test

Specimen Number	Flight Mean Load (FML) [% CSAI]	Maximum Compressive Flight Load [% CSAI]	N Number of Blocks (Number of Cycles)	Impact-Induced Damage Growth	RCS [MPa]
33F1	30%	78%	8 (3,200,000)*	yes	-
31A5	30%	78%	10 (4,000,000)	yes	499
31A6	30%	78%	10 (4,000,000)	yes	534
33F2	27.5%	72%	10 (4,000,000)	yes	-
33F5	27.5%	72%	10 (4,000,000)	no	448
33E6	27.5%	72%	10 (4,000,000)	no	474
31F1	25%	65%	10 (4,000,000)	no	-
33F6	25%	65%	10 (4,000,000)	no	410
31A7	25%	65%	10 (4,000,000)	no	512

* indicates failure

Modified-Spectrum Test (Two Lowest Load Levels Omitted)

Specimen Number	Flight Mean Load (FML) [% CSAI]	Maximum Compressive Flight Load [% CSAI]	N Number of Blocks (Number of Flights)	Impact-Induced Damage Growth	RCS [MPa]
33C4	30%	78%	10 (40,000)	yes	441
31D2	30%	78%	10 (40,000)	yes	503
33C2	30%	78%	10 (40,000)	yes	-
33C5	27.5%	72%	10 (40,000)	yes	478
31D6	27.5%	72%	10 (40,000)	no	538
33E7	27.5%	72%	10 (40,000)	yes	-
33E2	25%	65%	10 (40,000)	no	472
31E4	25%	65%	10 (40,000)	no	487
31F5	25%	65%	10 (40,000)	no	-

TABLE 9. CRITICAL STRAIN ENERGY RELEASE RATES FOR AS4/3501-6

Mode I G_{Ic} [N/m]	Mode II G_{IIc} [N/m]	Reference
123 - 246	-	Davies and Benzeggagh[38]
175	460	Tian and Swanson[39]
110	605	Dahlen and Springer[40]

TABLE 10. TEST MATRIX FOR IMPACTED SPECIMENS

Loading Type	Variation	Number of Specimens
Static	Compression	5
	Tension	5
Constant-Amplitude C-C	- 4 load levels - 2 specimens per level	4 x 2
Constant-Amplitude T-T	- 3 load levels - 2 specimens per level	3 x 2
Constant-Amplitude T-C	- 3 load levels - 2 specimens per level	3 x 2
Full TWIST (@10 Hz) Compression dominated	- 1 flight mean load level - 3 specimens per level	1 x 3
Modified TWIST (@10 Hz) Compression dominated	- 2 flight mean load levels - 3 specimens per level (deletion of 2 lowest load levels)	2 x 3
Modified TWIST (@10 Hz) Tension dominated	- 2 flight mean load levels - 3 specimens per level (deletion of 2 lowest load levels)	2 x 3
	Total number of specimens	45

TABLE 11. TEST MATRIX FOR CENTER-HOLED SPECIMENS

Loading Type	Variation	Number of Specimens
Static	Compression Tension	5 5
Constant-Amplitude C-C	- 7 load levels - 3 specimens per level	7 x 3
Constant-Amplitude C-C stress ratio effect (R)	- 3 load levels - 2 specimens per level	3 x 2
Constant-Amplitude T-T	- 4 load levels - 3 specimens per level	4 x 3
Full TWIST (@10 Hz) Compression dominated	- 3 flight mean load levels - 3 specimens per level	3 x 3
Modified TWIST (@10 Hz) Compression dominated	- 3 flight mean load levels - 3 specimens per level (deletion of 2 lowest load levels)	3 x 3
Modified TWIST (@10 Hz) Tension dominated	- 3 flight mean load levels - 3 specimens per level (deletion of 2 lowest load levels)	3 x 3
	Total number of specimens	76